ENHANCED INTERFACES AND TRAIN CATEGORIES FOR DYNAMIC COMPATIBILITY ASSESSMENT OF EUROPEAN RAILWAY BRIDGES

D2.2 – Worst-case combination of critical parameters of existing bridges

DELIVERABLE INFORMATION	
Work package number:	WP2
Work package title:	Identification of critical bridge parameters for the assessment of the economic impact of the new DTCs
Deliverable number:	D2.2
Deliverable title:	Worst-case combination of critical parameters of existing bridges
Due date of deliverable:	30-04-2026
Actual submission date:	08-04-2026
Responsible partner:	UdS
Revision:	
Dissemination level:	PU

This project has received funding from the Europe's Rail Joint Undertaking under Horizon Europe research and innovation programme under grant agreement No. 101121765 (HORIZON-ER-JU-2022-ExplR-02).

PUBLICATION HISTORY

Revision	Date	Description	Responsible
1.0	08-04-2026	Initial version	P. Galvín/UdS

Project Consortium

Coordinator

Universidade do Porto
UPORTO, Portugal

Beneficiaries

Kungliga Tekniska Hoegskolan
KTH, Sweden

Universidad Politecnica de Madrid
UPM, Spain

Bundesanstalt Fuer Materialforschung Und –Pruefung
BAM, Germany

Deutschen Bahn InfraGO AG
DB, Germany

Acoustique Et Vibrations Logiciels Scientifiques
AVLS, France

Affiliated Partners (to UPM)

Universitat Politecnica de Valencia
UPV, Spain

Universitat Jaume I de Castellon
UJI, Spain

Universidad de Sevilla
UdS, Spain

Administrador de Infraestructuras Ferroviarias
ADIF, Spain

Associated Partner

University Of Huddersfield
HUD, UK

Acknowledgments: This project has received funding from the Europe's Rail Joint Undertaking under Horizon Europe research and innovation programme under grant agreement No. 101121765 (HORIZON-ER-JU-2022-ExplR-02).

TABLE OF CONTENTS

1 Introduction

The development of a Single European Railway Area is a key objective of Europe's Rail Joint Undertaking (EU-Rail), aiming to harmonize standards and improve interoperability across Europe. A critical challenge in this initiative is to enhance the structural analysis of railway bridges to optimize capacity, service quality and cost efficiency. Railway bridges play a fundamental role in rail transport networks, yet their dynamic response under operating conditions remains a complex issue requiring advanced methodologies for accurate assessment.

InBridge4EU project `https://inbridge4eu.eu/` started on September 1st 2023. The project is funded by EU-Rail under Horizon Europe research and innovation program. The overall objective of InBridge4EU is to develop a dynamic interface between railway bridges and rolling stock, proposing new methods compatible with existing regulations, namely INF TSI [1], LOC&PAS TSI [2], EN 15528 [3], EN 1990-Annex A2 [4] and EN 1991-2 [5], and approaching the analysis of existing infrastructures, which role is critical for the sustainability of the European rail system. The project is structured into seven work packages, the second of which is devoted to identifying the critical parameters that govern the vertical acceleration of the deck, ultimately related to traffic safety.

During the first year of the project, with the support of five railway Infrastructure Managers, an extensive and representative set of European railway bridges from 11 conventional and High-Speed (HS) lines are selected. Main structural features, including technical drawings and project documents, are retrieved and stored in a database: `https://computeruse.us.es/`. Starting from the beginning of the second year, time-step calculation (TSC) transient dynamic analyses are performed over the complete database to obtain the bridges dynamic response under the circulation of 26 train models, selected based on their dynamic signature to be an envelope of more than 300 existing High-Speed trains across Europe. From the statistical analysis of these results, realistic worst-case combinations of critical parameters leading to the maximum vibrational response of the bridges are identified.

The database is a tool for the management of data generated within the project. It includes information on bridges, data from experimental tests and results from numerical analyses. The application was developed using `Python`. Data visualization is effectively achieved by means of both GET and POST methods, taking advantage of the capabilities of `Matlab`, `Python` and `Julia` for comprehensive analyses and visualisation. The implementation of a virtual private cloud ensures enhanced security measures. Users can securely access the system using user login credentials and API tokens, with group permissions facilitating control over access levels and functionalities.

The integration of large-scale databases and advanced computational techniques is currently redefining structural assessment and maintenance strategies for bridges [6]. In this context, Jesus et al. [7] presented a statistical analysis of the dynamic response of a railway viaduct concluding that key parameters cannot be analysed individually because in some cases interaction effects can be more important than single effects. Monti et al. [8] proposed a fully automated, model-free decision support system to assist railway operators in bridge safety management via real-time monitoring data. Regarding lifecycle management, Collings [9] evaluated data from both in-service and decommissioned structures to identify critical parameters for structural assessment. Other research has focused on specific structural components; for instance, Shen et al. [10] utilized a quasi-

static test database and physics-enhanced convolutional neural networks to estimate the bearing capacity of railway bridge piers. Similarly, Elnahla et al. [11] leveraged non-destructive evaluation data to establish a quantitative framework for predicting bridge deck deterioration. Complementarily, Bayane et al. [12] introduced a real-time approach for damage detection in operational bridges relying on five unsupervised anomaly detection algorithms. Furthermore, the use of extensive synthetic datasets has proven essential for complex dynamic studies, as demonstrated by Le Nguyen et al. [13], who employed a numerical database of over 10000 bridges for the generative design of High-Speed ballasted structures.

This paper presents a statistical analysis based on the bridge features and on the results of the numerical dynamic analyses conducted on the bridges documented in the database. The objective of this analysis is to identify realistic bridge parameter combinations within the database, determine the most critical parameters and their combinations that yield maximum vertical bridge accelerations during train passages, and characterize the statistical distribution of these critical parameters.

2 Data base

A preliminary evaluation of the bridge population reveals that 55 % of the structures present simply-supported (SS) spans, 15 % are continuous bridges, and 30 % are portal frames (Figure 1). Two types of culvert-like structures are analysed: closed portal frames, characterized by a continuous base slab (box culvert), and open portal frames, which consist of a top deck and lateral walls supported by independent footings. The frame configuration is characterized by a large-span deck rigidly connected to its supports. As per the main structural material, 28 % are prestressed concrete bridges, 25 % steel-concrete composite structures, and 4 % are steel bridges, with the remainder consisting of reinforced concrete. The most prevalent deck configuration is the full slab (40 %), followed by filler beam (22 %), beam (9 %), and U-girder decks (7.5 %). Furthermore, the sample is approximately evenly distributed between single-track and double-track configurations. Finally, 89 % of the analysed cases feature ballasted tracks.

2.1 Numerical analysis

All the bridges within the database are analyzed with either planar analytical or three-dimensional (3D) finite element (FE) numerical models. In the first case only longitudinal bending is accounted for and in the second, the 3D deformation of the bridge decks is considered. The computational procedure involves determining the structural dynamic response under several train passages in a wide speed interval ranging from 144 to 450 km/h in 1.8 km/h intervals, specifically assessing maximum vertical accelerations and displacements at the platform.

Damping values are assigned according to EN 1990-Annex A2 [4], based on the bridge material and span length.

The selection of the trains for the dynamic analyses is based on the concept of dynamic train signature, introduced by European Rail Research Institute (ERRI) [14]. This is a simplified method that enables the dynamic effects of different trains at resonance and away from resonance to be compared independently of the characteristics of the bridge. For simply-supported bridges and neglecting structural damping the

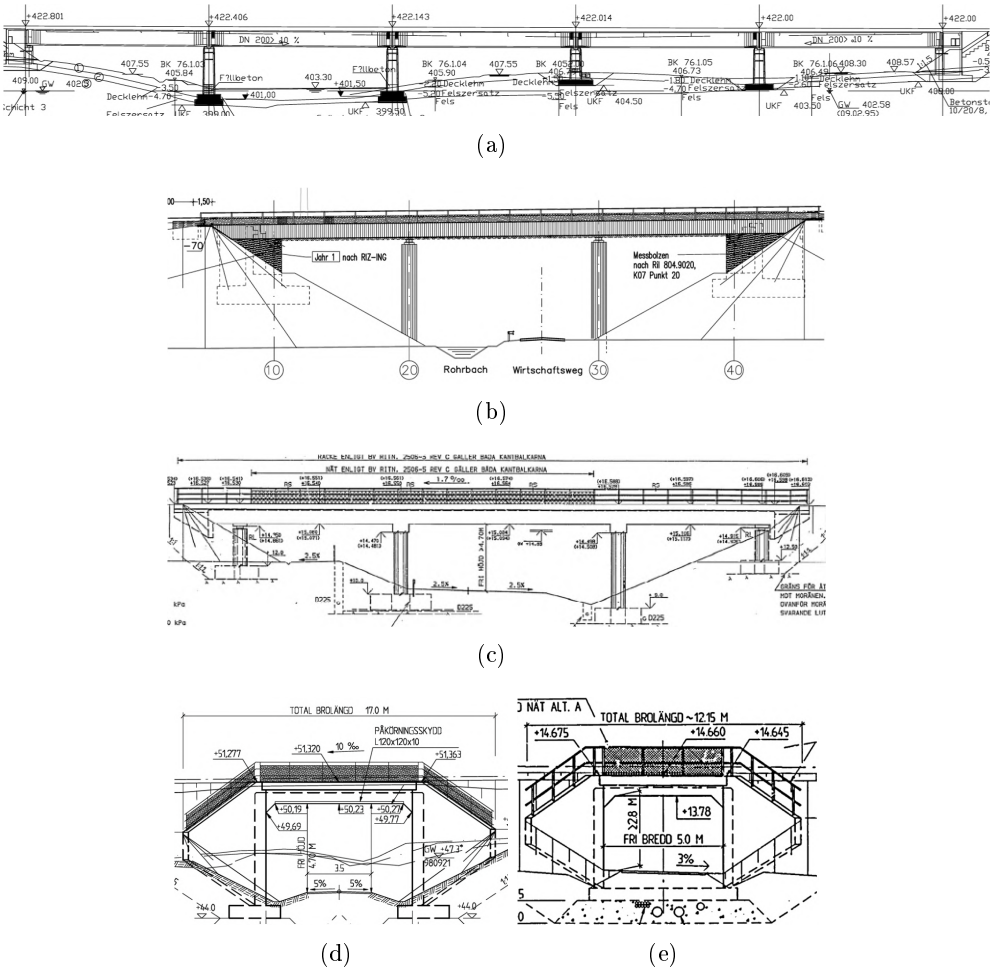

(a)

(b)

(c)

(d) (e)

Figure 1: Bridges longitudinal configurations: (a) simply-supported, (b) continuous, (c) frame, (d) open portal frame and (e) closed portal frame.

following expression is derived:

$$S_0(\lambda) = \max_{i=1,\dots,M} \sqrt{\left[\sum_{k=1}^{i} P_k \cos\left(\frac{2\pi x_k}{\lambda}\right)\right]^2 + \left[\sum_{k=1}^{i} P_k \sin\left(\frac{2\pi x_k}{\lambda}\right)\right]^2} \tag{1}$$

where i is the axle number and M the number of axles of the train, P_k is the axle load of the $k-$th axle, x_k the distance between the $k-$th axle and the first one, and λ the wavelength of excitation defined as v/n_0, where v is the train speed and n_0 the fundamental frequency of the bridge.

First, over 350 HS European real trains are selected from a passenger train database also developed within the InBridge4EU project as starting point, and their dynamic signatures are computed. Then, the signatures of the 10 High-Speed load model-A (HSLM-A) from Eurocode (EC) trains [5] are superimposed. It is a known fact that these artificial trains are no longer an envelope of the dynamic effects of some of the newest trains in Europe. Therefore, for the analyses performed herein a (not too large) subset of these real trains is selected with the aim of covering the HSLM-A gaps in the signature wavelengths.

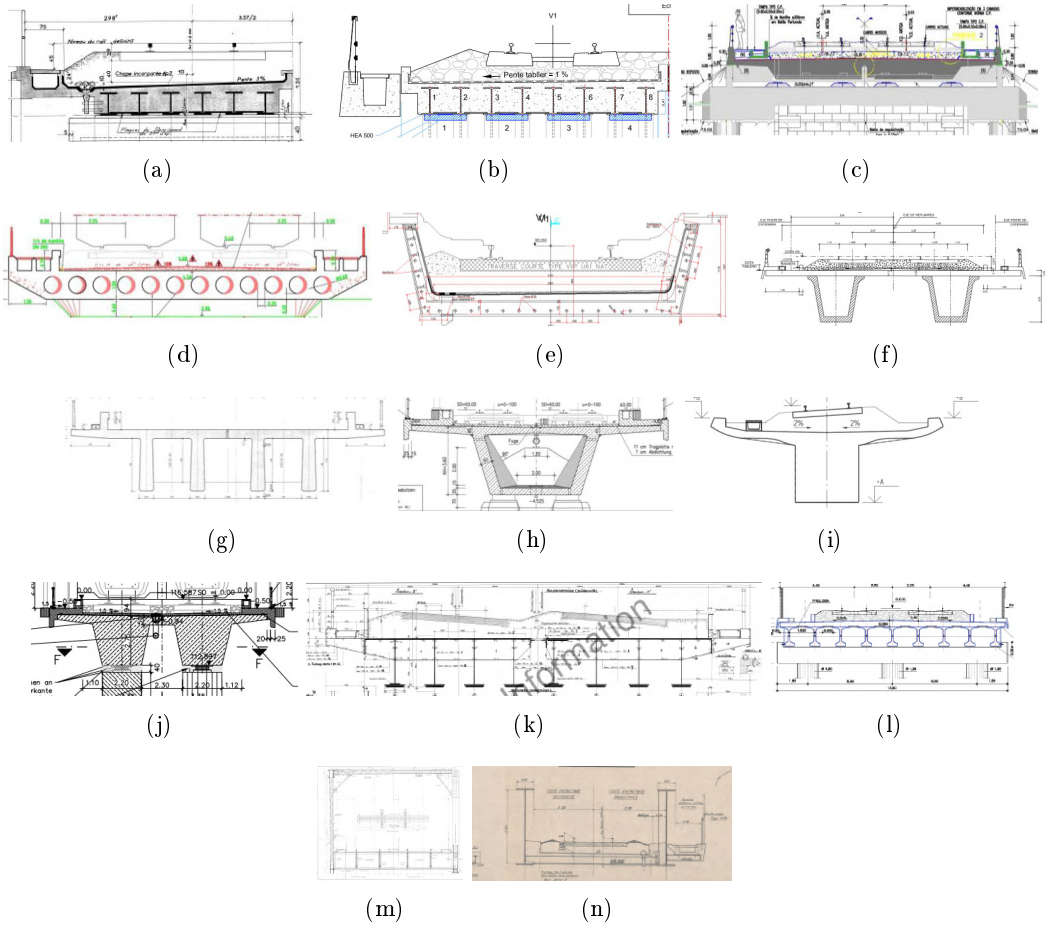

Figure 2: Schematic representation of the most common deck types analyzed: (a) filler beam, (b) reinforced filler beam, (c) full slab, (d) hollow slab, (e) U-type, (f) U-girder, (g) T-beam, (h) box-girder, (i) beam, (j) slab beam, (k) grillage, (l) multi-girder, (m) truss, and (n) half-through bridges.

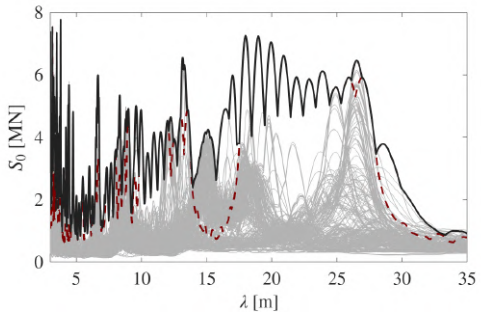

Figure 3: (Grey) Database HS trains, (dashed red) HSLM-A envelope and (black) envelope signatures of 10 HSLM-A + 16 trains final selection.

Figure 3 shows the real HS trains and the HSLM-A signatures. By an optimization process based on minimizing the normalized error relative to the HSLM-A signature 16

real trains are finally selected. These 16 trains and the 10 HSLM-A trains constitute an envelope of the dynamic signatures of the starting 350 trains in the database, as shown in the figure.

Given the number of bridges and the time-intensive nature of the dynamic simulations, the methodology prioritizes the use for the most computationally efficient models possible. Initially, three fundamental beam configurations are employed across all typologies of the 509 bridges included in the study: simply supported, continuous, and fixed-end beams. These Bernoulli-Euler analytical models are used to evaluate the serviceability limit state in a first stage in order to roughly differentiate the bridges that exhibit inadequate dynamic behaviour. Accordingly, only the longitudinal bending response of the structures is accounted for. Also, factors such as the deck obliqueness, supports flexibility and interaction with either the soil, the vehicle or the track are disregarded. It should be stressed that despite these simplifications the adopted models and analysis procedure are aligned with the standards recommendations.

Although simple models are used, time consuming can be high, mainly when long bridges are studied. For this reason, a new novel analytical method for computing the dynamic response of multi-span railway non-uniform beams with general boundary conditions, subjected to moving loads, based on time-discrete analysis using sinc interpolation has been developed by the authors and applied in this work. The method admits modal superposition by transforming the convolution integrals of normal coordinates into time integrals of trigonometric functions. The methodology is implemented in the SINC-Dyn function package [15]. Alternatively, CALDINTAV [16], a user-friendly software application designed for the dynamic analysis of railway bridges subjected to high-speed train loadings, can be used.

In a second stage, 3D FE models are developed for the 94 bridges that failed to meet the acceleration compliance criteria during the initial beam-based analysis (maximum acceleration of $5\,\mathrm{m/s^2}$ and $7.5\,\mathrm{m/s^2}$ in ballasted and non-ballasted tracks, respectively). The approach has been to implement detailed models for all non-compliant bridges to perform modal analyses and extract the lowest natural frequencies and mode shapes along the load paths (rails) and at the response post-processing points. These modal parameters are subsequently utilized in time-step calculation (TSC) dynamic analyses to obtain the bridges dynamic response under the train models previously mentioned employing the SINC-Dyn toolbox [15]. In all instances, only the superstructure is modelled; the stiffness and deformation of piers, abutments, and foundations are disregarded. The particular shell/solid modelling approach varies according to the deck typology. The linear mass of each deck, as specified in the database, is strictly maintained. Furthermore, non-structural masses (comprising ballast, sleepers, rails, sidewalks, etc.) are uniformly distributed over the platform area. These masses are adjusted to ensure that the 3D FE models and their corresponding analytical beam counterparts maintain identical total mass properties.

3 Statistical analysis

This section presents a statistical analysis based on the computed results. For bridges where vibration levels remained below the established threshold using simplified models, those initial results were retained (415 bridges). Conversely, in cases requiring more complex structural modelling, the computations derived from these advanced models were utilized for the subsequent analysis (94 bridges).

3.1 Data analysis, structural parameters and parameter interdependence

In general, portal frame bridges are predominant for short spans ($L < 10\,\text{m}$). Owing to the short span and the rigid connection between the deck (typically a full slab) and the abutments, these structures exhibit significantly higher natural frequencies than simply supported or continuous bridges. In addition, they present higher bending stiffness than other typologies. In the long-span range ($L > 30\,\text{m}$), both simply supported and continuous bridges are commonly found. Although the natural frequencies are relatively low due to the large spans, the linear mass is generally high (over $20000\,\text{kg/m}$). This is associated with the structural typologies typical of this span range, such as U-girder or box-girder bridges. The stiffness requirements for these spans result in very massive structures, which are unlikely to experience significant accelerations, even under resonance conditions. The intermediate span range ($10\,\text{m} < L < 30\,\text{m}$) concentrates a large number of bridges with relatively low linear masses and natural frequencies. Many of these bridges are simply supported, with slab bridges and filler beam decks being predominant. Within this span range, continuous bridges generally present higher linear masses. It is within this span range that greater dynamic problems can be expected.

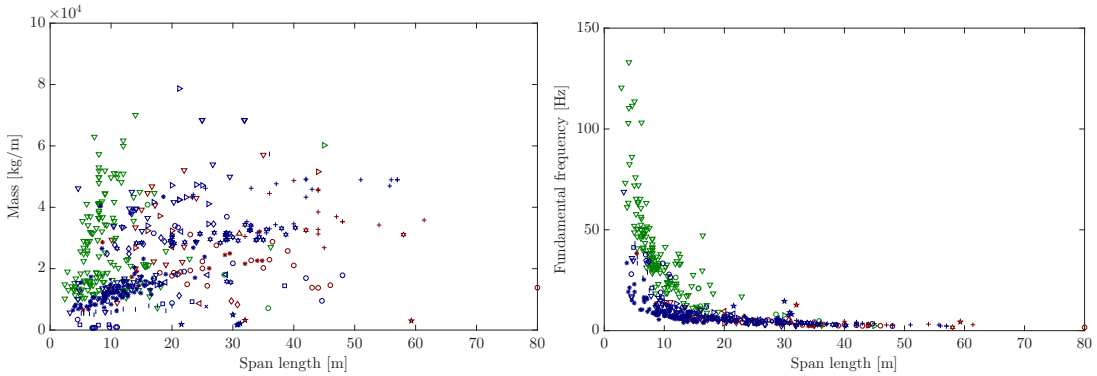

(a) (b)

Figure 4: Distribution of (a) mass per unit length and (b) fundamental frequency versus maximum span length: (red) continuous, (green) frame, portal frame open and portal frame closed, and (blue) simply-supported bridge configurations. Markers represent deck types: ○: beam, +: box, ∗: filler beam, ·: filler beam reinforced, ×: grillage, □: half-through, ◇: multi-girder, △: beam slab, ▽: full slab, ▷: hollow slab, ◁: T beam, ⋆: truss, ⚹: U-girder deck, |:U-type deck.

Figure 5 illustrates the variation in the mass per unit length, fundamental frequency, bending stiffness index, damping ratio[5] and maximum predicted acceleration across different bridge configurations. In these plots, the horizontal blue line represents the median (50th percentile). The blue box is defined by the 25th and 75th percentiles, while the black whiskers indicate the dispersion outside this central 50% range. Circles denote outliers. While most configurations maintain a similar median mass, a significant outlier is observed in the portal frame open configuration; this specific case corresponds to an exceptional bridge carrying seven tracks. The fundamental frequencies for the portal frame type configurations are the highest and exhibit the greatest dispersion. Certain atypical values exceeding 100 Hz result from the numerical modelling assumptions, specifically the consideration of fully fixed boundary conditions.

Conversely, simply-supported and continuous bridges show lower, more concentrated fundamental frequency ranges. The bending stiffness index shown in Figure 5(c) is defined as EI/L^2, where EI denotes the bending rigidity (the product of Young's modulus and the area moment of inertia) and L represents the maximum span length. This parameter is directly related to the ratio of span length to the maximum displacement produced by a unit load. Portal frame bridges exhibit the highest median values, which are associated with the typical structural typologies adopted, most commonly full slabs. Finally, simply-supported bridges exhibit numerous outliers with accelerations exceeding $10\,\mathrm{m/s^2}$, indicating that this configuration is more susceptible to exhibiting substantial vibration levels associated to resonance phenomena.

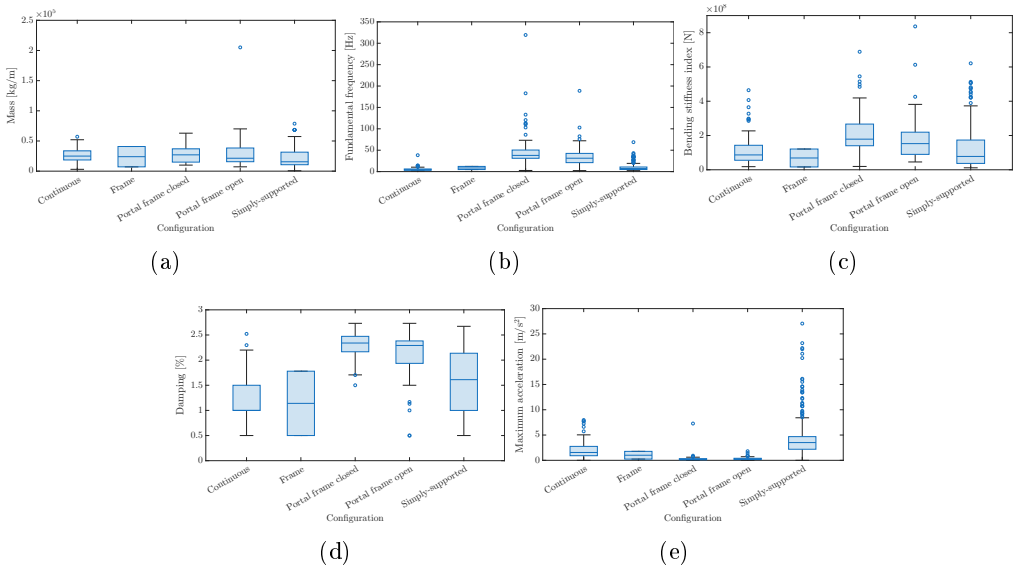

Figure 5: Statistical distribution of structural and dynamic parameters grouped by bridge longitudinal configuration: (a) linear mass, (b) fundamental frequency, (c) bending stiffness index, (d) damping[4], and (e) maximum vertical acceleration. Boxes represent the interquartile range, the horizontal line denotes the median, and circles indicate statistical outliers.

Figures 5(d) and 6 illustrate the influence of the damping ratios. These values are derived from EN 1990-Annex A2 [4] based on specific bridge properties; consequently, damping is treated as a dependent variable in the statistical analysis.

Figure 7 shows the structural and dynamic response of the bridge dataset, discretized into ten fundamental frequency intervals ranging from $(1, 5]$ Hz to $(30, 40]$ Hz. There is a discernible, although non-linear, trend where mass tends to stabilize or slightly decrease as the fundamental frequency increases. This is consistent with structural dynamics, as higher frequencies often correspond to shorter spans or stiffer cross-sections with lower total mass per length. Lower fundamental frequency bridges exhibit substantially higher bending stiffness index values. Low frequencies ($f_1 < 5\,\mathrm{Hz}$) are generally associated with high mass and high stiffness. This is typically the case for long-span bridges ($L > 30\,\mathrm{m}$), which, due to stiffness requirements, especially in HS lines, are usually constructed with stiff and massive sections; consequently, acceleration levels are generally not expected to be significant. At the other end of the spectrum, in the high-frequency range ($f_1 > 18\,\mathrm{Hz}$), although the linear mass may be relatively low, acceleration levels

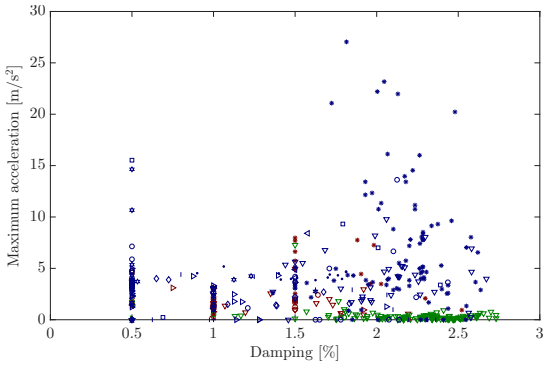

Figure 6: Distribution of maximum vertical acceleration versus damping values: (red) continuous, (green) frame, portal frame open and portal frame closed, and (blue) simply-supported bridge configurations. Markers represent deck configurations: ○: beam, +: box, ∗: filler beam, ·: filler beam reinforced, ×: grillage, □: half-through, ◇: multi-girder, △: slab beam, ▽: slab full, ▷: slab hollow, ◁: T beam, ⋆: truss, ⚹: U-girder deck, |:U-type deck.

are also not excessive because these bridges usually correspond to structural types such as frame bridges with very high flexural stiffness. The most critical situation occurs in the intermediate frequency range (between 5 and 12 Hz), where both stiffness and mass tend to be low. This is typical of simply supported slab and filler beam bridges with short-to-medium spans. On average, the bridges that exhibit the highest acceleration levels fall within this frequency range and are characterized by low linear masses and low bending stiffness.

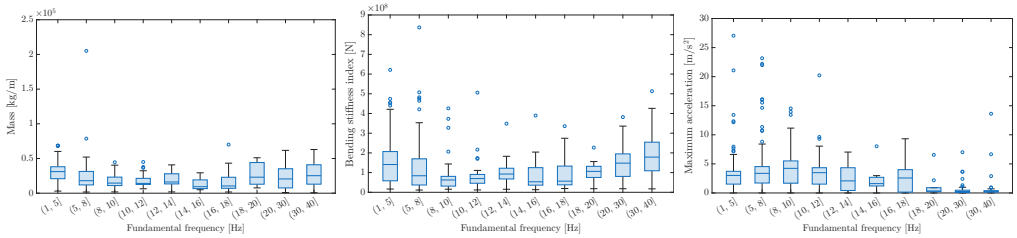

(a) (b) (c)

Figure 7: Boxplot analysis of bridge parameters discretized by fundamental frequency intervals: (a) distribution of mass, (b) bending stiffness, and (c) maximum acceleration.

The interdependence between structural parameters and the resulting maximum acceleration is now evaluated through a Pearson correlation analysis. To ensure the reliability of the observed trends, a significance test is performed, masking all correlations with a p-value exceeding 0.05 (Figure 8). A statistically significant negative correlation is observed between the fundamental frequency and the maximum acceleration. This confirms that higher structural stiffness -and the consequent shift to higher frequency ranges- effectively reduces the susceptibility to resonant vibration under train passages. A strong, significant positive correlation exists between mass and bending stiffness index. This dependency is physically consistent with bridge design trends, where larger cross-sections required for higher load-bearing capacity inherently increase both linear mass and cross-section inertia. The significant positive correlation between the oper-

ational maximum velocity V_{max} and mass/bending stiffness index suggests that lines designed for higher operational speeds are typically associated with more robust structural typologies. Figure 8 clarifies that deck type, bending stiffness index and material are the primary categorical drivers of the fundamental frequency, whereas parameters like skewness show impact on the global peak acceleration. It should be indicated that the skewness is not included in the simplified analyses due to their planar nature but it is included in the ones performed with 3D FE models. Fundamental frequency, bending stiffness index, mass, material and longitudinal configuration are the primary drivers of peak acceleration, with the highest values concentrated in simply-supported bridges and those exhibiting natural frequencies below 10 Hz.

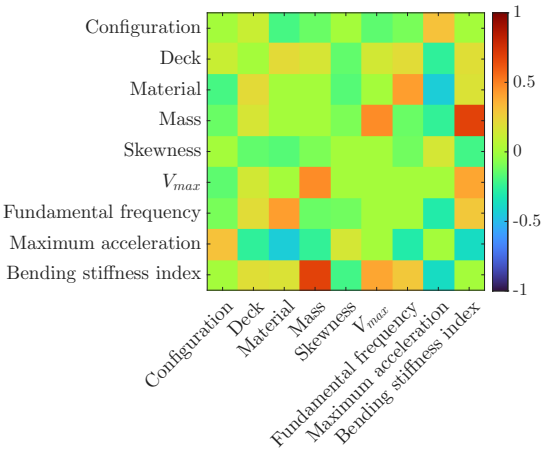

Figure 8: Full Pearson correlation matrix (R) retaining only coefficients with a p-value < 0.05. Non-significant relationships are masked (set to zero) to highlight robust structural dependencies.

The analysis reveals that while fundamental frequency remains the universal driver for all typologies, the impact of structural mass and stiffness is highly configuration-dependent, with simply-supported spans showing the greatest sensitivity to resonance-induced accelerations. Next, a category-specific correlation analysis is performed to isolate the mechanical drivers of peak acceleration for each bridge longitudinal configuration, revealing that the influence of structural parameters is highly dependent on this factor.

An analysis is performed exclusively on the simply-supported dataset, evaluating the interdependence of different deck types on the mass, bending stiffness index, frequency, and acceleration levels (Figure 9). The linear mass distribution exhibits significant fluctuations depending on the deck typology. Hollow and full slab bridges show the highest mass dispersion, whereas truss and U-type decks present the most lightweight and consistent profiles. The fundamental frequency is highly sensitive to the deck selection. While beam and U-type decks are present in a broad frequency range, box and U-girder deck configurations are concentrated in the lower frequency bands, as they are usually used for long spans. A critical finding is observed in the filler beam deck category. Despite having moderate mass and frequency medians, this deck type produces the most severe acceleration outliers. The acceleration levels of filler beam decks identify them as high-priority candidates for advanced monitoring in rail networks. The box deck typologies exhibit the highest median values and broadest dispersion for the bending stiffness index. In contrast, filler beam and half-through decks show significantly lower

and more concentrated stiffness, which correlates with their highest accelerations.

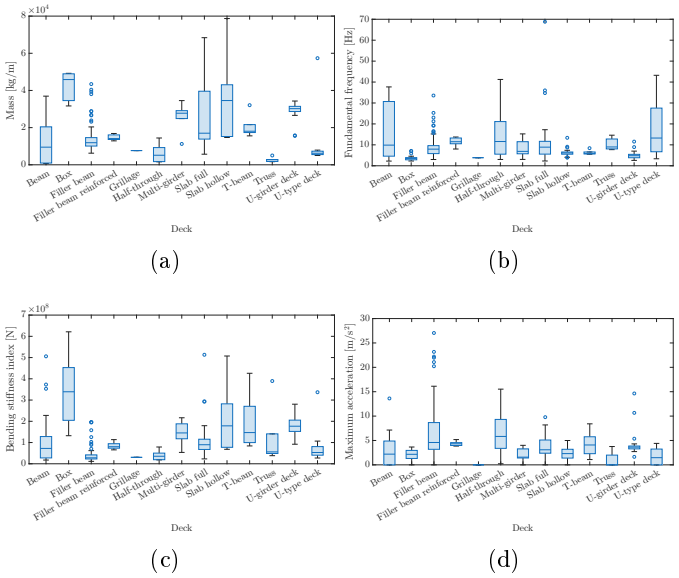

Figure 9: Comparative analysis of structural parameters for the simply-supported bridge population categorized by deck typology: (a) linear mass, (b) fundamental frequency, (c) bending stiffness index, and (d) maximum vertical acceleration.

The distribution of structural parameters into fundamental frequency bins (Figure 10) shows a clear inverse relationship between bending stiffness and fundamental frequency, where the highest EI/L^2 values are associated with the lowest frequencies, typical of long-span bridges (see Figure 4). While mass generally decreases as frequency increases, significant outliers are noted in the $8-12\,\mathrm{Hz}$ range representing specific short-span deck typologies. Peak vertical accelerations exhibit a drastic increase in both magnitude and dispersion within the lower frequency spectrum, specifically between 1 and 10 Hz. Above the $16-18\,\mathrm{Hz}$ threshold, the median acceleration stabilizes significantly below $5\,\mathrm{m/s^2}$, suggesting that stiffer structures are inherently less susceptible to resonant excitation from train passages.

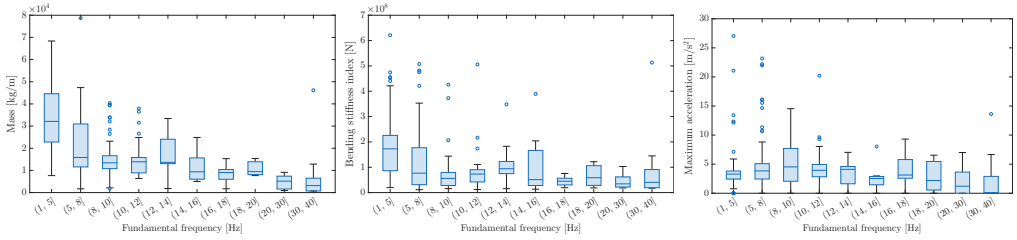

Figure 10: Distribution of bridge mass, peak vertical acceleration, and bending stiffness across fundamental frequency bins for the simply-supported bridge population.

The correlation matrix for simply-supported bridges (Figure 11) reveals that geometric parameters such as skewness are less influential than other factors; instead, the dynamic response is governed by a significant interaction between mass, bending stiffness index, material, deck type, operational velocity, and fundamental frequency.

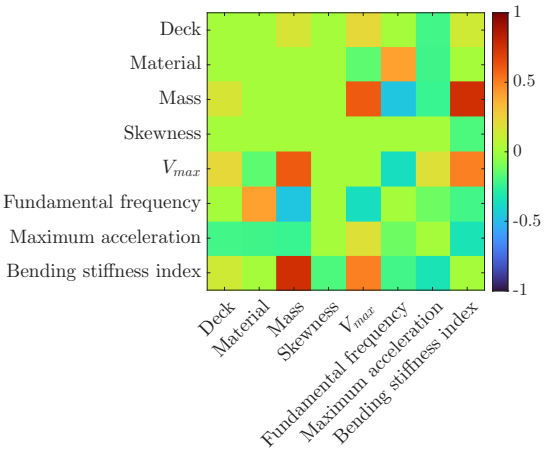

Figure 11: Full Pearson correlation matrix (R) for the simply-supported bridge population retaining only coefficients with a p-value < 0.05. Non-significant relationships are masked (set to zero) to highlight robust structural dependencies.

The influence of the deck type on the dynamic behaviour of continuous bridges shows a more stable response compared to the previous configuration. Figure 12 shows that, unlike SS spans, continuous bridges maintain accelerations consistently below $5\,\mathrm{m/s^2}$, suggesting that structural redundancy effectively reduces the acceleration levels.

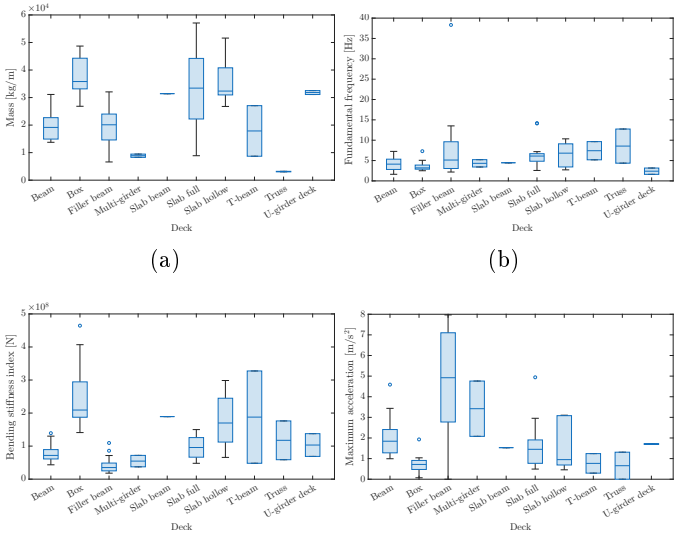

Figure 12: Comparative analysis of structural parameters for the continuous bridge population categorized by deck typology: (a) linear mass, (b) fundamental frequency, (c) bending stiffness index, and (d) maximum vertical acceleration.

The relationship between frequency and structural parameters confirms the general robustness of continuous bridges when compared to SS cases (Figure 13). The highest mass values are associated with the lowest frequency bin ($1 - 5\,\mathrm{Hz}$). As the frequency increases, the mass stabilizes at lower values, indicating a transition toward lighter structural typologies. The bending stiffness index remains fairly constant across the

full frequency range. Figure 13(c) highlights that continuous bridges do not experience the remarkable acceleration levels previously showed in flexible simply-supported spans. Even at low frequencies, the maximum acceleration remains controlled, demonstrating that continuity mitigates resonance risks.

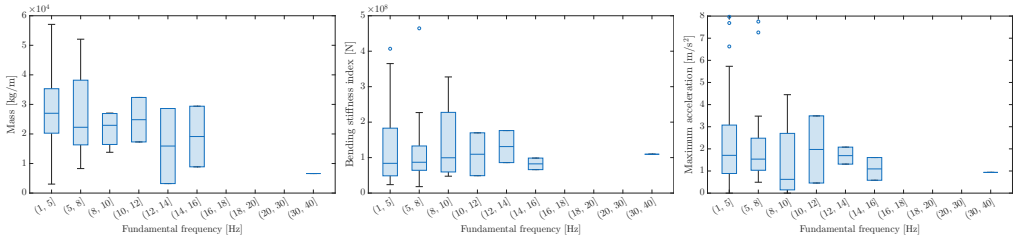

(a) (b) (c)

Figure 13: Distribution of bridge mass, peak vertical acceleration, and bending stiffness across fundamental frequency bins for the continuous bridge population.

The significant correlation matrix for continuous bridges (Figure 14) shows a significant departure from the behaviour of simply-supported spans, most notably the statistical decoupling between fundamental frequency and maximum acceleration. While in simply-supported bridges the fundamental frequency is the main predictor of the dynamic risk, in continuous configurations, it leaves to be a reliable indicator. This phenomenon can be attributed to (i) in continuous bridges, the hyperstatic system allows vibration energy to be distributed across the full structure rather than concentrating at one span, (ii) the continuity of the deck which provides higher internal damping and more complex load paths, effectively mitigate resonance amplifications (this is evidenced in Figure 13(c), where accelerations remain consistently low even for bridges in the low-frequency range), and (iii) low frequency modes with closely spaced natural frequencies contribute to the response which is not governed by the fundamental mode unlike in the simply-supported case. Consequently, for HS railway bridge design, continuous bridges constitute a much more robust alternative.

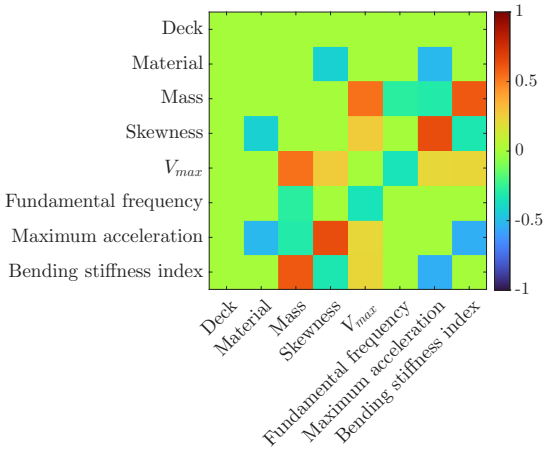

Figure 14: Full Pearson correlation matrix (R) for the continuous bridge population retaining only coefficients with a p-value < 0.05. Non-significant relationships are masked (set to zero) to highlight robust structural dependencies.

Frame bridges group -including frames and both open and closed portal frames- represent the most rigid typology in the dataset. It should be noted that only beam-type analyses have been performed on frames due to their very low dynamic response. Figure 15 shows that these structures are characterized by low vertical accelerations, with almost all cases falling below $2\,\mathrm{m/s^2}$ unlike in simply-supported or continuous bridges. The distribution of structural parameters across frequency bins (Figure 16) shows that linear mass and bending stiffness remain constant up to 10 Hz. For frequencies above this threshold, the bending stiffness index increases significantly as span lengths decrease.

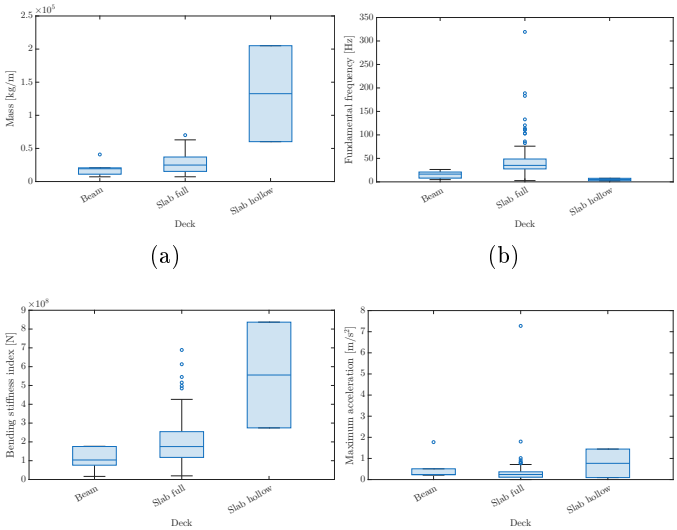

Figure 15: Comparative analysis of structural parameters for the frame bridge population categorized by deck typology: (a) linear mass, (b) fundamental frequency, (c) bending stiffness index, and (d) maximum vertical acceleration.

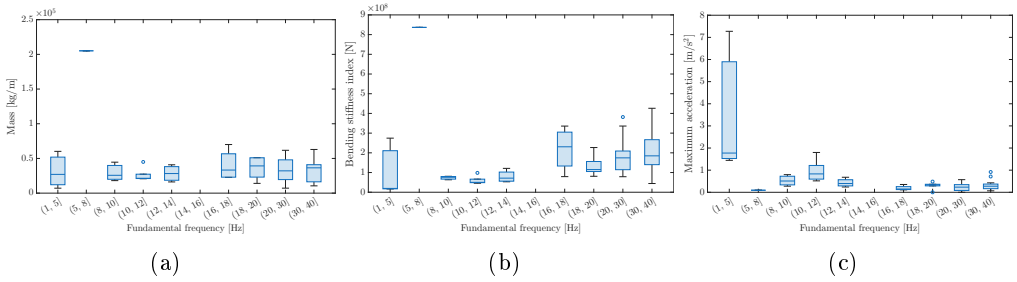

Figure 16: Distribution of bridge mass, peak vertical acceleration, and bending stiffness across fundamental frequency bins for the frame bridge population.

The significant correlation matrix for the frame population (Figure 17) reveals a highly decoupled dynamic system. The statistical analysis shows that maximum acceleration is almost independent of most structural and geometric parameters, including deck type and fundamental frequency, and that there is a strong coupling between bending stiffness, mass, and fundamental frequency, which is expected in monolithic reinforced concrete structures. Frame bridges provide enough rigidity and damping, with a relevant participation of soil radiation, to prevent significant energy transfer from the

train to the structure, resulting in a low acceleration response.

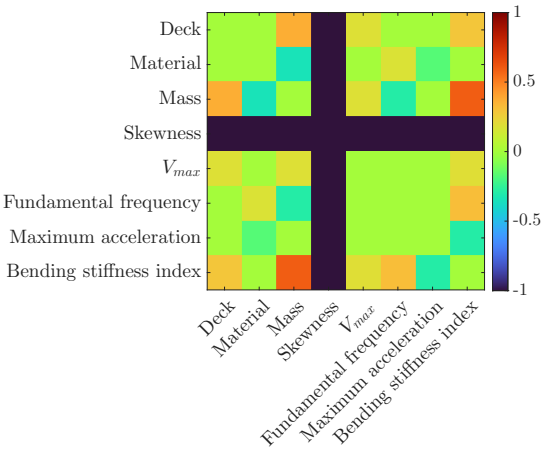

Figure 17: Full Pearson correlation matrix (R) for the frame bridge population, which contains no skew bridges, retaining only coefficients with a p-value < 0.05. Non-significant relationships are masked (set to zero) to highlight robust structural dependencies.

3.2 Stepwise linear regression model

Following the data analysis, a Stepwise Linear Regression (SLR) model is implemented to quantify the influence of the identified structural parameters. The model follows an approach based on the Bayesian Information Criterion (BIC), ensuring that only statistically significant variables are retained to prevent overfitting. The performance of the SLR is initially evaluated using the entire dataset (Figure 18(a, b)). This global model yields an R^2 of 0.3793 and a Root Mean Square Error ($RMSE$) of 2.8585 $\mathrm{m/s^2}$. To ensure the robustness of the baseline linear model, a diagnostic analysis is conducted using studentized residuals and Cook's distance. Observations with $|r_{stud}| > 3$ are flagged as outliers, while influential points are identified using a Cook's distance threshold of $4/n$, where n is the total number of observations. Figure 18 reveals several bridges exceeding this limit. By removing these anomalous data points (Figure 18(c, d), the performance of the model significantly improves, reaching an R^2 of 0.4815 and the $RMSE$ reducing to 1.7692 $\mathrm{m/s^2}$. To ensure a valid comparison between the different stages of the model, the residual distributions are presented as Probability Density Functions (PDF). In these plots, the area under the histogram is normalized to unity, making the distributions comparable regardless of the number of observations in each subset. This diagnostic phase is useful, as it filters out noisy data -such as bridges with very high mass-to-stiffness ratios or resonant peaks- that could otherwise bias the subsequent machine learning models.

The SLR is applied individually to each bridge longitudinal configuration to assess the linearity of their dynamic responses (Figures 19, 20, 21). Simply-supported bridges constitute the biggest prediction challenge, with an initial R^2 of only 0.3116. After eliminating outliers, R^2 improves to 0.3401. The relatively low accuracy and high $RMSE$ (2.2565 $\mathrm{m/s^2}$) confirm that resonant situations in SS bridges are highly non-linear with the fundamental frequency to train speed ratio and make it difficult to capture the response with standard regression models. Continuous bridges show better alignment with linear assumptions. The refined model achieves an R^2 of 0.4565 and a notably lower $RMSE$ of 1.0427 $\mathrm{m/s^2}$. The more concentrated residual histogram suggests that the structural redundancy of continuous bridges leads to a more easily predictable dynamic behaviour. Frame bridges initially show an R^2 of 0, indicating that the predictors had no linear relationship with the very low accelerations of these bridges. After removing outliers, the model reached an R^2 of 0.3511 with a low $RMSE$ of 0.1723 $\mathrm{m/s^2}$. This confirms that for frames, the acceleration level is consistently low and effectively decoupled from the main structural parameters.

The linear analysis demonstrates that while the SLR is effective for identifying general trends and cleaning the dataset, it is insufficient for precise acceleration prediction, particularly for the simply-supported bridges. The persistent dispersion in the residuals indicates that complex interactions between mass, fundamental frequency, and maximum operational speed require a non-linear approach. Consequently, a random forest regression model is proposed in the following subsection to better capture these high-order dependencies.

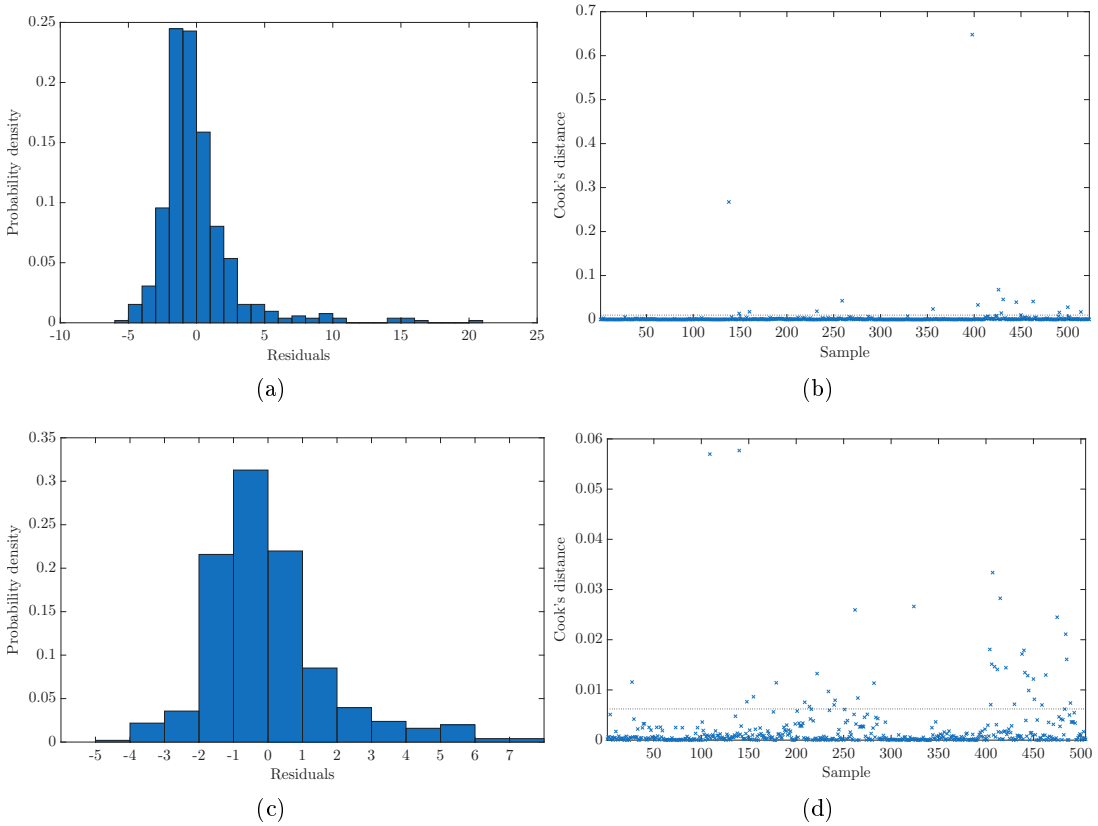

Figure 18: Diagnostic analysis of the global linear model using (a,b) the full dataset ($R^2 = 0.3793$ and $RMSE = 2.8585\,\mathrm{m/s^2}$) and (c,d) after removing identified outliers and influential points ($R^2 = 0.4815$ and $RMSE : 1.7692\,\mathrm{m/s^2}$): (a,c) histogram of raw residuals showing the initial error distribution and (b,d) Cook's distance plot identifying influential observations. The Cook's distance threshold is plotted by dashed lines.

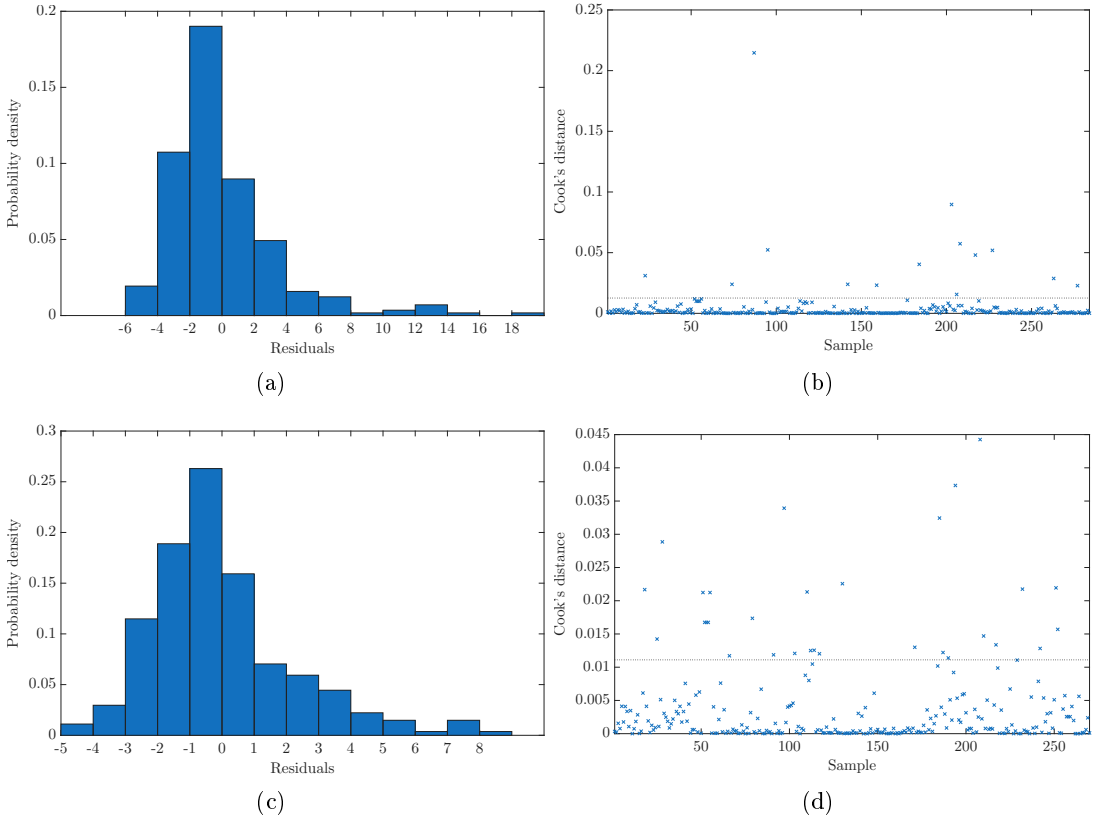

Figure 19: Diagnostic analysis of the linear model using (a,b) the full dataset for the simply-supported bridge population ($R^2 = 0.3116$ and $RMSE = 3.4388\,\mathrm{m/s^2}$) and (c,d) after removing identified outliers and influential points ($R^2 = 0.3401$ and $RMSE = 2.2565\,\mathrm{m/s^2}$): (a,c) histogram of raw residuals showing the initial error distribution and (b,d) Cook's distance plot identifying influential observations.

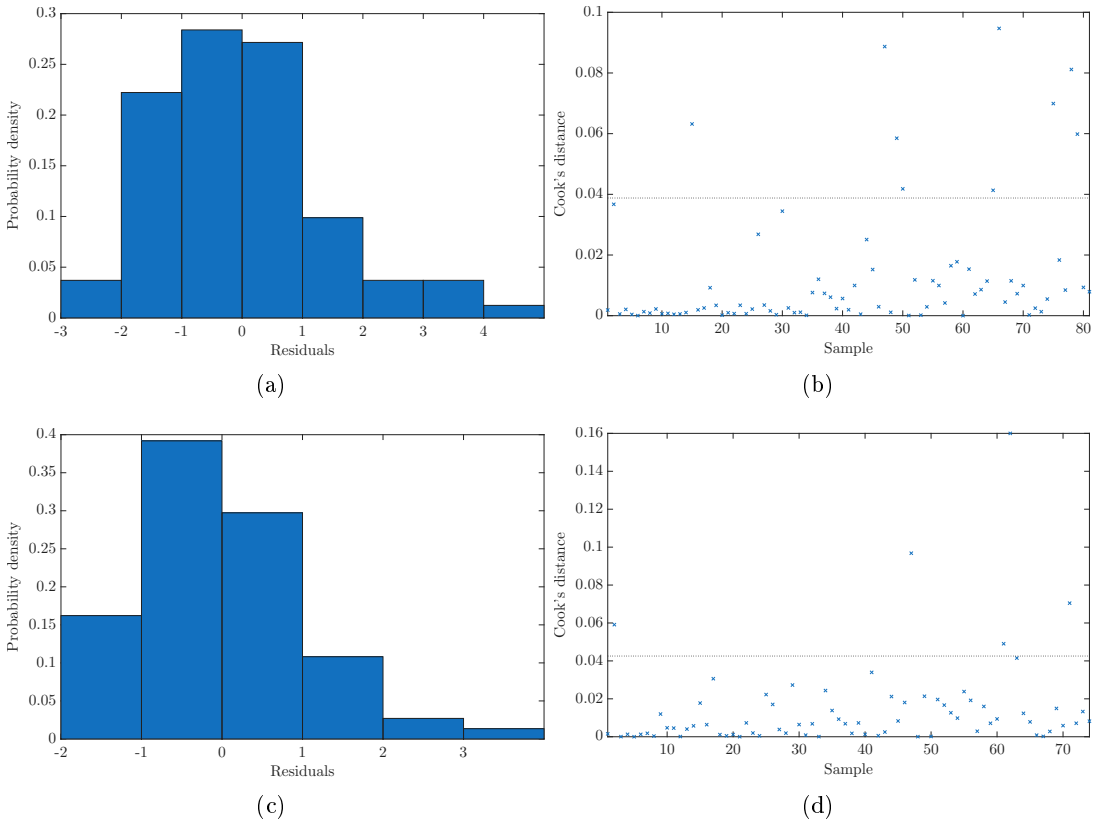

Figure 20: Diagnostic analysis of the linear model using (a,b) the full dataset for the continuous bridge population ($R^2 = 0.4228$ and $RMSE : 1.4556\,\mathrm{m/s^2}$) and (c,d) after removing identified outliers and influential points ($R^2 = 0.4565$ and $RMSE : 1.0427\,\mathrm{m/s^2}$): (a,c) histogram of raw residuals showing the initial error distribution and (b,d) Cook's distance plot identifying influential observations.

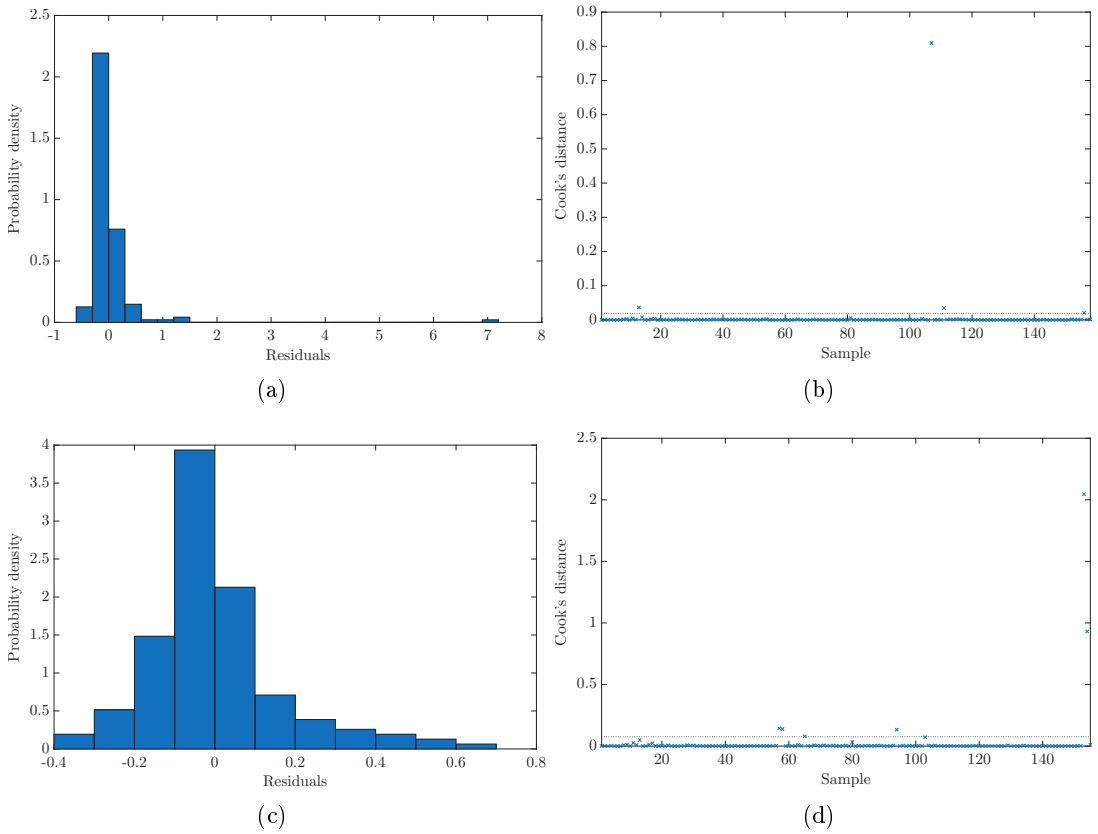

Figure 21: Diagnostic analysis of the linear model using (a,b) the full dataset for the frame bridge population ($R^2 = 0$ and $RMSE : 0.6181\,\mathrm{m/s^2}$) and (c,d) after removing identified outliers and influential points ($R^2 = 0.3511$ and $RMSE : 0.1723\,\mathrm{m/s^2}$): (a,c) histogram of raw residuals showing the initial error distribution and (b,d) Cook's distance plot identifying influential observations.

3.3 Random forest regression model and machine learning

To overcome the inherent non-linearity of resonance phenomena that linear models fail to capture, a Random Forest (RF) regression model is developed using a Gradient Boosting approach (LSBoost). Unlike standard black-box models, the RF is enhanced through physical feature engineering, introducing a synthetic parameter to the predictor set: Dimensionless speed = $V_{max}/(2Ln_0)$ (a non-dimensional parameter relating maximum operational velocity (V_{max}), maximum span length (L), and fundamental frequency (n_0) to quantify the characteristic speed-frequency ratio [17]).

The model is trained on 80% of the dataset, leaving 20% for independent testing. To ensure robustness and prevent overfitting, Bayesian Optimization is employed to fine-tune the hyperparameters using a 5-fold cross-validation scheme. The search space is constrained to a minimum leaf size of 5 to ensure that the model learned general physical trends rather than memorizing individual bridge samples. The RF model achieved high predictive accuracy, with an R^2 of 0.8770 and an $RMSE$ of 0.9440 $\mathrm{m/s^2}$ on the unseen test set (Figure 22). As shown in Figure 22(a), most observations fall within a ±20% interval, indicating a strong capture of the dynamic response. The Residual Probability Density (Figure 22(b)) shows a zero-centered distribution with a high concentration of errors near zero. The fat-tailed nature of the distribution (where the theoretical normal curve is wider than the central histogram peak) highlights that while the model is highly accurate for the majority of the population, a few cases, physically complex to predict, account for the largest errors.

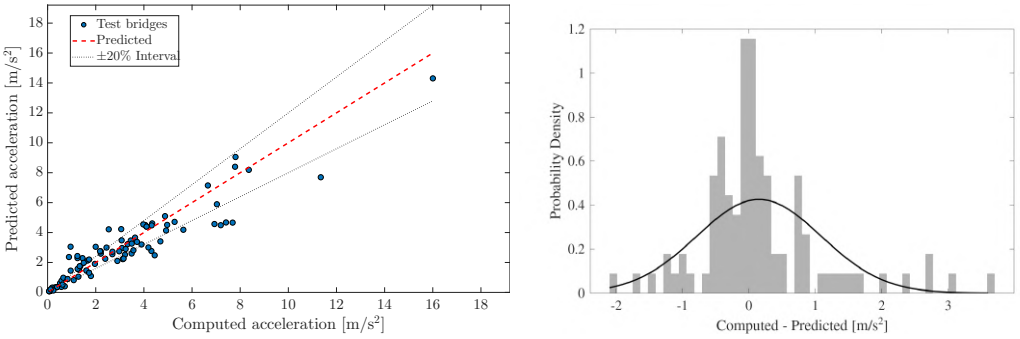

Figure 22: Performance of the optimized Random Forest model on the test set: (a) Predicted vs. computed acceleration with ±20% confidence intervals and (b) probability density of residuals.

To evaluate the contribution of each structural and operational parameter to the dynamic response of the bridge, a predictor importance analysis is performed (Figure 23). Furthermore, the complex non-linear relationships captured by the RF model are visualized using Partial Dependence Plots (PDP) and Individual Conditional Expectation (ICE) curves (Figure 24). The importance analysis reveals that the longitudinal configuration of the bridge is the most influential factor, followed closely by the dimensionless speed. This hierarchy indicates that the model successfully prioritizes the structural typology and the dimensionless ratio that governs the dynamic interaction regime over individual variables like mass or stiffness. The high ranking of the dimensionless speed summarizes the interaction between geometry, frequency, and speed. Mass and bending stiffness show moderate importance, acting as secondary parameters of the acceleration amplitude. Figure 24 provides a detailed view of the physics learned

by the model. Regarding the maximum operational speed, the standard PDP shows a stepped increase in acceleration, while the ICE curves reveal that for certain bridges, there are sharp jumps at specific speeds, indicating that the model has identified individual resonant situations. The dimensionless speed analysis shows a clear upward trend. The Partial Dependence Plots reveal non-linear staircase increments in acceleration as the factor approaches critical thresholds. This behaviour, observed in individual ICE curves, represents the physical transition at resonance, a phenomenon that the random forest model captures without an explicit closed-form dynamic equation. The stabilization of the median (blue line) below the mean (black line) suggests that while most bridges follow a steady trend, a subset of high-acceleration cases (outliers) increases the average. The model correctly identifies that increasing the mass or bending stiffness index of the bridge reduces the expected vertical acceleration, following an inverse non-linear relationship. Finally, for the fundamental frequency, the sensitivity is higher in the low-frequency range, where the highest accelerations are obtained, becoming almost neutral for very stiff structures.

An observation in the interpretability analysis is the presence of non-linear jumps or steps in acceleration at specific dimensionless speed values. While the dimensionless speed is calculated using the maximum operational velocity (V_{max}), resonance does not necessarily takes place at such speed. High accelerations are triggered when any of the excitation frequencies, produced by the periodic passage of axles or bogies, coincides with any of the bridge natural frequencies. Since the dataset records the maximum acceleration reached across the entire speed range $[0, V_{max}]$, a bridge will exhibit a high response if a critical resonant speed with relevant amplitude is less than or equal to V_{max}. In this context, V_{max} acts as a scanning envelope; if the resonant threshold is within the operational speed range, the peak acceleration is captured. The specific steps observed at sub-multiples of the main resonance peak suggest that the random forest model identifies multiple resonance orders (harmonics). The model ability to identify these jumps at specific factor values demonstrates that it has not only learned a statistical correlation but has effectively mapped the spectral limit states and the underlying dynamic behaviour of the structures.

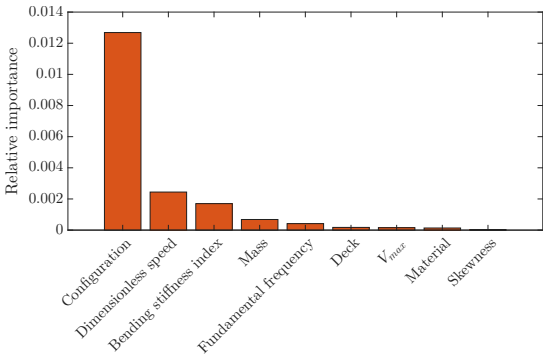

Figure 23: Relative importance of predictors for the complete bridge set.

The limitations of traditional statistical methods for predicting complex dynamic responses are evident when comparing the linear regression results with the random forest model. As shown in Figure 18, the global linear model achieved a modest $R^2 = 0.3793$ with a significant error ($RMSE = 2.8585\,\mathrm{m/s^2}$). Even after removing outliers, the linear model only reached $R^2 = 0.4815$. In contrast, the optimized RF model (Figure 22)

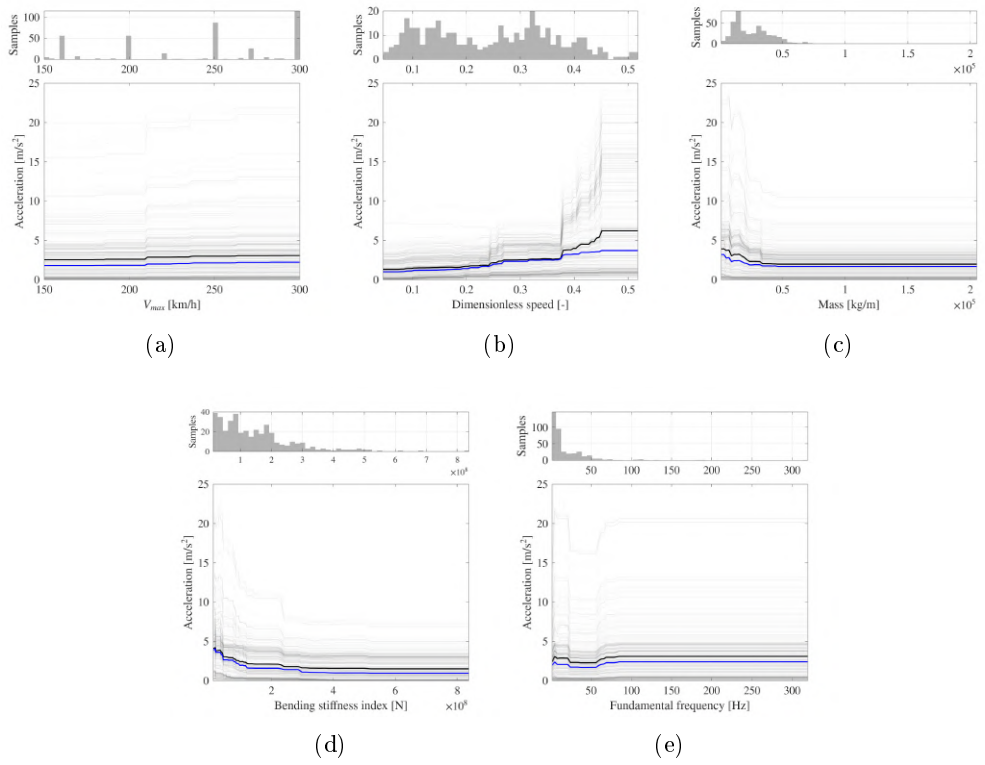

Figure 24: Interpretability analysis of the random forest model for the complete bridge set. (a-e) Partial Dependence Plots (PDP) and Individual Conditional Expectation (ICE) curves for key predictors. The thick black line represents the average global trend (mean PDP), the blue line indicates the median response (robust trend), and the grey lines show individual bridge sensitivities (ICE). Top histograms illustrate the sample density across the training range.

achieved an $R^2 = 0.8770$ and an $RMSE$ of $0.9440\,\mathrm{m/s^2}$ on unseen data. The SLR residuals (Figure 18(a)) show a wide, asymmetrical distribution, indicating that the model systematically fails to capture high-acceleration events. However, the RF residuals are centred around zero, demonstrating that the ensemble approach significantly reduces both bias and variance compared to the linear approach.

The fundamental deficiency of the linear model lies in its assumption of proportionality. In railway bridge dynamics, acceleration does not increase linearly with speed or frequency; instead, it exhibits sudden peaks due to resonance. Figures 18-21 show that even when segmented by configuration (simply-supported, continuous, or frame), the linear models consistently lead to R^2 values below 0.5. The RF model, through the introduction of the dimensionless speed, effectively linearises the problem and, while the SLR model treats speed as a simple multiplier, the RF model identifies it as part of a trigger mechanism for resonant conditions, as seen in the non-linear jumps of the ICE curves. The comparative analysis suggests that while linear models can provide a rough estimation of average behaviour, they are unreliable for applications in railway engineering. The RF model acts as an accurate surrogate that can identify the resonance response of the bridges. The transition from $R^2 \approx 0.50$ (LR) to $R^2 \approx 0.88$ (RF) represents a shift from a simple statistical fit to a model that mimics the underlying

structural behaviour.

The performance of the Random Forest model was further scrutinized by segmenting the dataset into structural configurations (Table 1 and Figures 25–33). This sub-analysis reveals critical insights into the dynamic behaviour of each typology.

Simply-supported bridges exhibited the highest $RMSE$ ($2.9625\,\mathrm{m/s^2}$), consistent with their high susceptibility to resonance. Predictor importance for this group (Figure 26) highlights that, apart from the dimensionless speed, mass plays a key role, acting as the primary inertial moderator of the response.

Continuous bridges showed the most balanced performance ($R^2 = 0.6811$), where the bending stiffness index emerged as a significant predictor in this configuration.

Frame structures presented an R^2 of 0.8154 and achieved the lowest absolute error $RMSE = 0.0710\,\mathrm{m/s^2}$. This result is explained by the high stiffness of frame configurations. These structures experience very low accelerations with minimal dispersion. It is important to note that the frame category encompasses three distinct sub-configurations: open frames, closed frames, and simple frames. Despite this internal geometric variety, the model achieved its highest absolute precision in this category.

Across all cases, the dimensionless speed and bending stiffness index remained the top-ranked predictors, proving that the proposed physical feature engineering is a good descriptor of the dynamic risk regardless of the bridge longitudinal configuration. These results confirm that the global model benefits from learning the cross-categorical boundaries, while the individual models highlight the specific physical drivers of each structural type.

Table 1: Performance metrics of the Random Forest model disaggregated by structural configuration.

Configuration	$RMSE$ ($\mathrm{m/s^2}$)	R^2
Simply-supported	2.9625	0.5858
Continuous	1.0213	0.6811
Frame	0.0710	0.8154
Global Model	0.9440	0.8770

The findings of this study demonstrate that the optimized Random Forest model, enhanced by physical feature engineering, serves as an accurate surrogate for predicting the dynamic response of railway bridges. In engineering practice, this model can be implemented as a robust screening tool for large-scale infrastructure assessment. By utilizing the dimensionless speed as a primary performance indicator, engineers could rapidly identify bridges at risk of exceeding acceleration limits without the need for computationally expensive time-history simulations. The methodology allows for a two-tier management approach: i) Fast Screening: the model filters thousands of bridge configurations in seconds using only basic geometric and operational data, flagging resonant-prone structures, and ii) Targeted Analysis: resources for complex dynamic analyses can then be focused exclusively on these flagged cases, significantly reducing the overhead costs and time of railway maintenance programs.

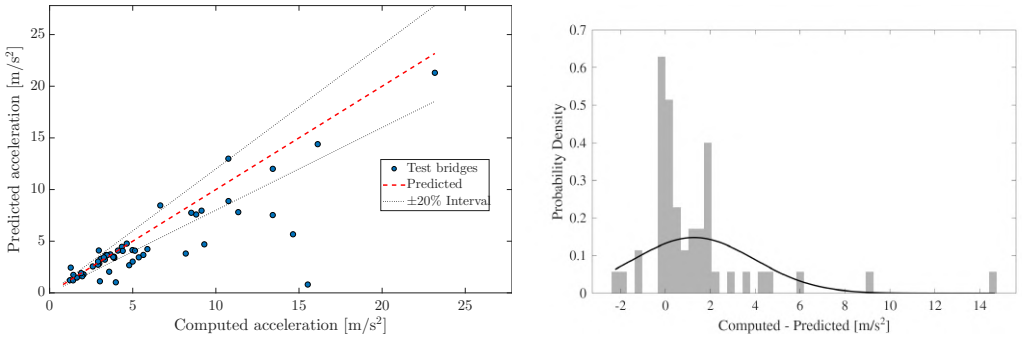

Figure 25: Performance of the optimized Random Forest model for the simply-supported bridge population on the test set: (a) Predicted vs. Actual acceleration with ±20% confidence intervals and (b) probability density of residuals.

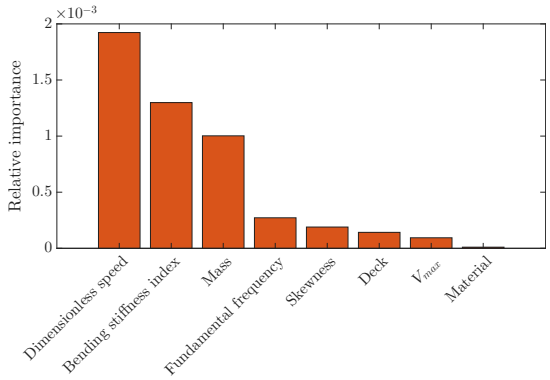

Figure 26: Relative importance of predictors of the random forest model for the simply-supported bridge population.

3.4 Analysis over a synthetic 1M bridge population: Deck performance evaluation

A synthetic sample of one million bridges is generated within the parameter range of the existing database. Using the predictive model, the maximum acceleration induced by the 26 train passages is obtained and the influence of various parameters is studied by categorizing the bridges according to their longitudinal configuration and deck typology. In the following figures, the color scale is saturated at $5\,\mathrm{m/s^2}$, which corresponds to the threshold considered acceptable for serviceability in ballasted tracks railway bridges.

Figures 34 to 36 present the maximum vertical acceleration results for the synthetic population categorized into three increasing mass intervals ($m_1 - m_2$, $m_2 - m_3$, and $m_3 - m_4$) where m_1 and m_4 are the minimum and maximum values respectively, and m_2 and m_3 are the 33^{th} and 66^{th} percentiles of the dataset. These heatmaps permit evaluating the dynamic response across different parameter spaces: bending stiffness index and fundamental frequency versus dimensionless speed, and fundamental frequency versus bending stiffness index. The distribution shows a clear critical red zone associated with specific combinations of low stiffness and high dimensionless speeds. Furthermore, the transition across the mass intervals reveals how increased bending stiffness index shifts these regions, generally expanding the stable operational zones as the mass per unit length of the deck increases. The critical zones are predominantly concentrated in the

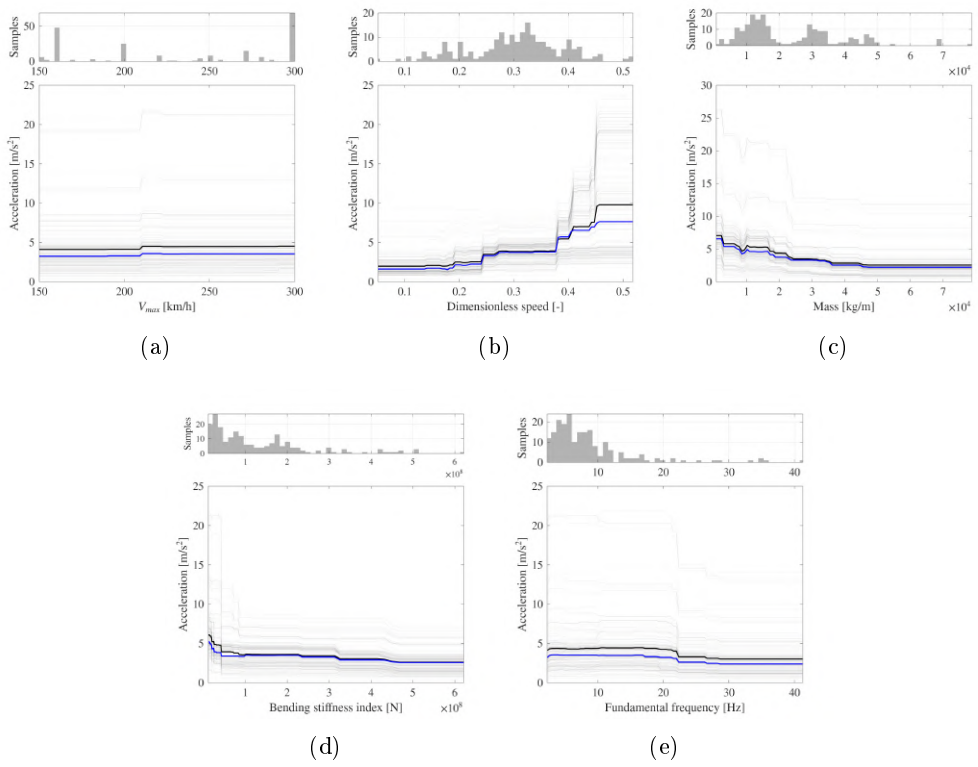

Figure 27: Interpretability analysis of the random forest model for the simply-supported bridge population. (a-e) Partial Dependence Plots (PDP) and Individual Conditional Expectation (ICE) curves for key predictors. The thick black line represents the average global trend (mean PDP), the blue line indicates the median response (robust trend), and the grey lines show individual bridge sensitivities (ICE). Top histograms illustrate the sample density across the training range.

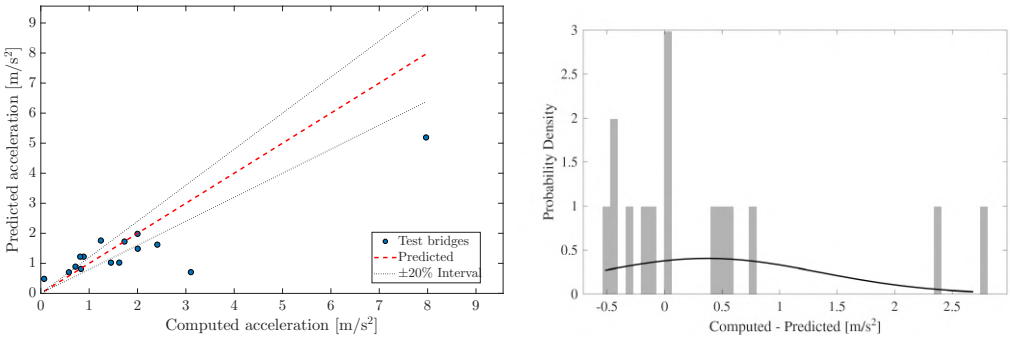

Figure 28: Performance of the optimized Random Forest model for the continuous bridge population on the test set: (a) Predicted vs. Actual acceleration with ±20% confidence intervals and (b) probability density of residuals.

lowest fundamental frequency range (< 5 Hz) when combined with high dimensionless speeds. In the lowest mass interval, the maximum acceleration consistently remains within the saturated red zone across almost the full fundamental frequency range. This indicates that for bridges in the lowest mass range, the structural mass becomes the

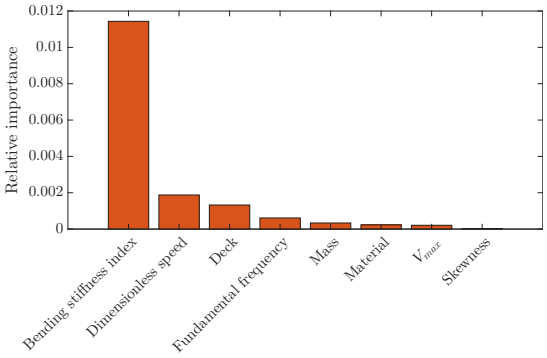

Figure 29: Relative importance of predictors of the random forest model for the continuous bridge population.

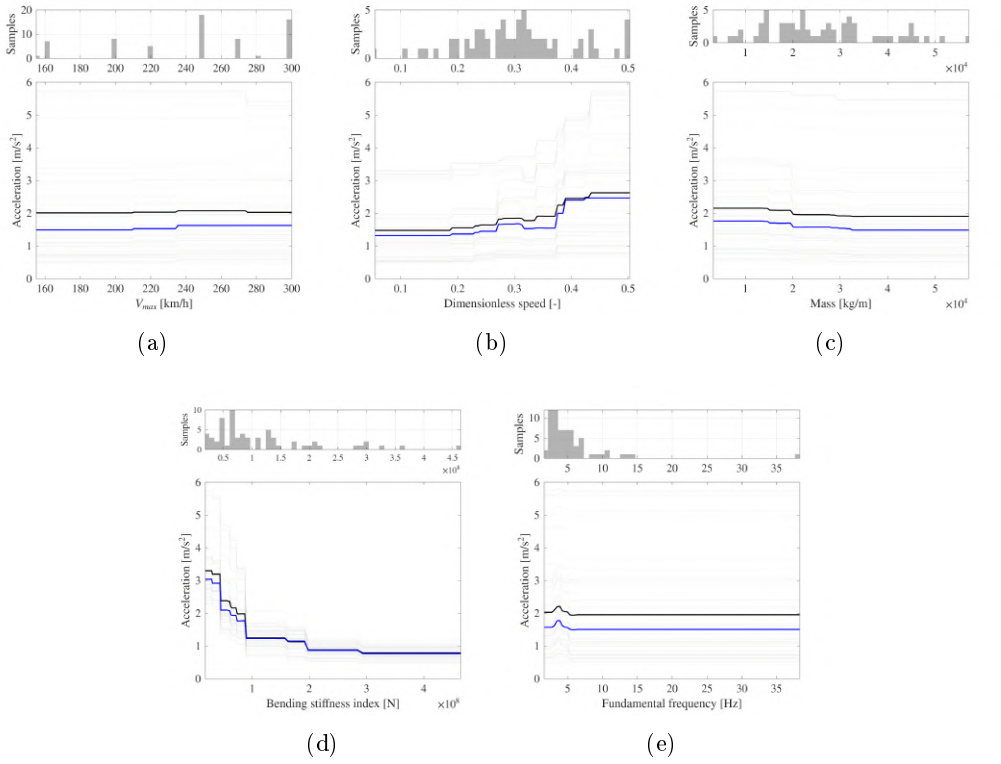

Figure 30: Interpretability analysis of the random forest model for the continuous bridge population. (a-e) Partial Dependence Plots (PDP) and Individual Conditional Expectation (ICE) curves for key predictors. The thick black line represents the average global trend (mean PDP), the blue line indicates the median response (robust trend), and the grey lines show individual bridge sensitivities (ICE). Top histograms illustrate the sample density across the training range.

governing factor of the dynamic response. In this regime, the system lacks sufficient mass to attenuate the energy induced by the train passage, leading to serviceability limit exceedances even when the the fundamental frequency is far from the resonance condition. In Figure 36, the interaction between fundamental frequency and the bending stiffness index reveals that a low fundamental frequency does not always lead to

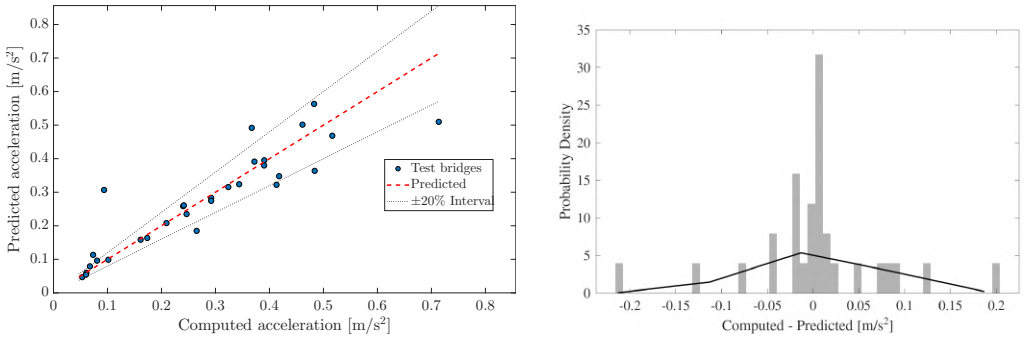

Figure 31: Performance of the optimized Random Forest model for the frame bridge population on the test set: (a) Predicted vs. Actual acceleration with ±20% confidence intervals and (b) probability density of residuals.

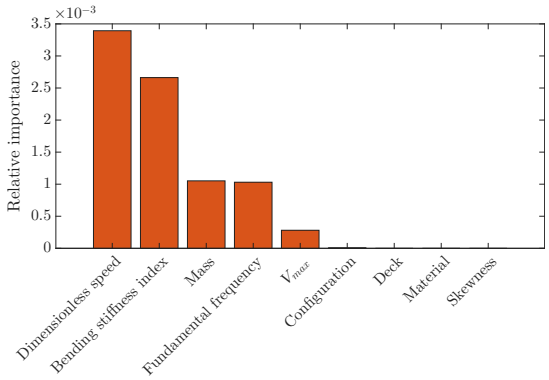

Figure 32: Relative importance of predictors of the random forest model for frame bridge population.

exceedance; however, when a low fundamental frequency coincides with low stiffness, the bridge enters the saturated acceleration zone. As the mass interval increases (moving from $m_1 - m_2$ to $m_3 - m_4$), these critical areas shift, demonstrating how the mass of the deck redefines the resonance boundaries associated with the bridge fundamental frequency.

Figure 37 provides a comprehensive parametric sensitivity and coupling analysis for the full subset of simply-supported bridges. These maps show how the maximum vertical acceleration is influenced by the interaction of structural properties and operational speed: Figure 37(a) confirms that low-mass decks ($< 2 \times 10^4\,\mathrm{kg/m}$) are extremely sensitive to speed even at low dimensionless speeds. As mass increases, the threshold speed at which the $5\,\mathrm{m/s^2}$ limit is exceeded shifts progressively to higher values. Figure 37(b) shows that at low dimensionless speeds only specific frequency ranges trigger high accelerations, but as the dimensionless speed increases beyond 0.3, the acceleration becomes critical across almost the complete frequency spectrum. Figure 37(c) shows a clear boundary: a lack of mass can be partially compensated for by very high stiffness, but there is a quadrant with low mass and low stiffness where serviceability is not met. Figure 37(d) shows a map relating fundamental frequency and mass predominantly saturated, particularly in the lowest mass region.

Figure 38 shows the distribution of maximum vertical accelerations for simply-supported bridges, categorized by deck typology, as a function of their mass per unit

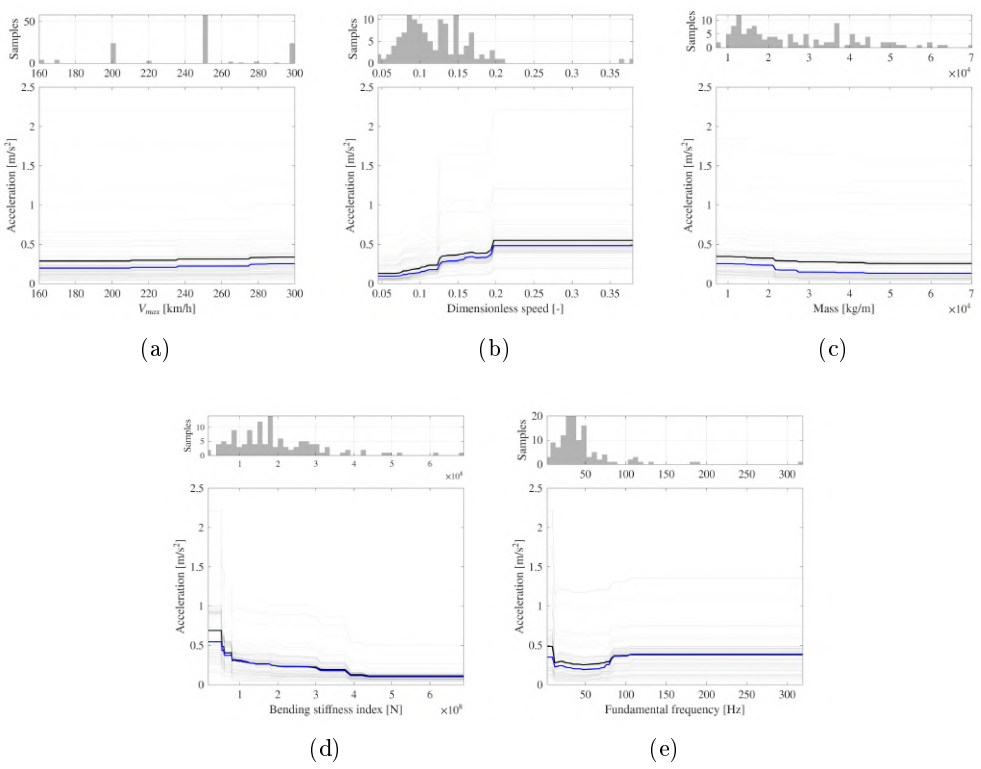

Figure 33: Interpretability analysis of the random forest model for the frame bridge population. (a-e) Partial Dependence Plots (PDP) and Individual Conditional Expectation (ICE) curves for key predictors. The thick black line represents the average global trend (mean PDP), the blue line indicates the median response (robust trend), and the grey lines show individual bridge sensitivities (ICE). Top histograms illustrate the sample density across the training range.

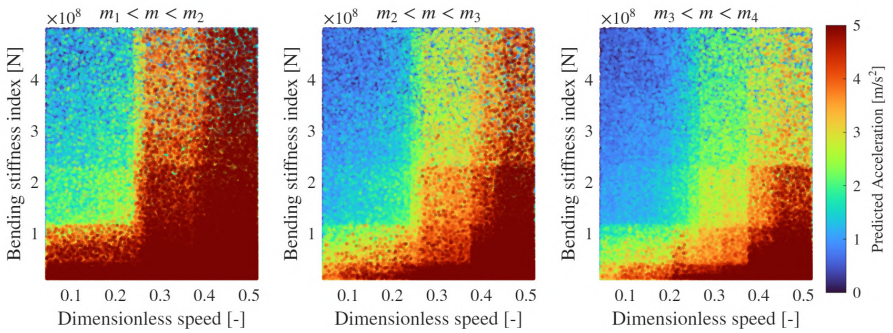

Figure 34: Parametric analysis of predicted vertical acceleration as a function of dimensionless speed and bending stiffness. The data is categorized into three mass per unit length intervals defined by the following thresholds: $m_1 = 711$, $m_2 = 7079$ (33^{rd} percentile of the dataset), $m_3 = 13446$ (66^{th} percentile of the dataset), and $m_4 = 20000\,\mathrm{kg/m}$. The color scale is saturated at $5\,\mathrm{m/s^2}$ to highlight configurations exceeding the maximum acceleration limit.

length and bending stiffness index. The background scatter plot represents the synthetic

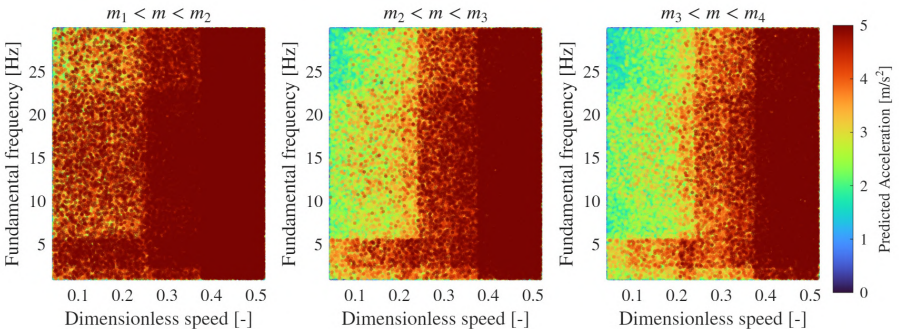

Figure 35: Parametric analysis of predicted vertical acceleration as a function of dimensionless speed and fundamental frequency. The data is categorized into three mass per unit length intervals defined by the following thresholds: $m_1 = 711$, $m_2 = 7079$ (33^{rd} percentile of the dataset), $m_3 = 13446$ (66^{th} percentile of the dataset), and $m_4 = 20000\,\mathrm{kg/m}$. The color scale is saturated at $5\,\mathrm{m/s^2}$ to highlight configurations exceeding the maximum acceleration limit.

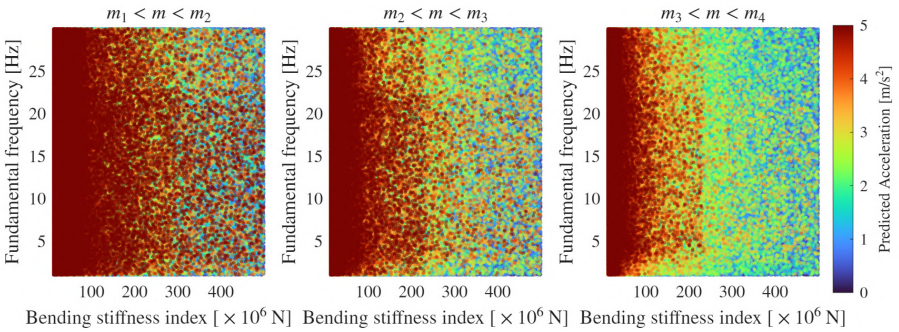

Figure 36: Parametric analysis of predicted vertical acceleration as a function of fundamental frequency and bending stiffness. The data is categorized into three mass per unit length intervals defined by the following thresholds: $m_1 = 711$, $m_2 = 7079$ (33^{rd} percentile of the dataset), $m_3 = 13446$ (66^{th} percentile of the dataset), and $m_4 = 20000\,\mathrm{kg/m}$. The color scale is saturated at $5\,\mathrm{m/s^2}$ to highlight configurations exceeding the maximum acceleration limit.

population, while the black lines indicate the mean values of the actual bridges in the database. The shaded grey area delimits the range defined by the mean ± one standard deviation, providing a visual benchmark of where existing structures stand relative to the critical acceleration zones. A comparative analysis across typologies reveals distinct safety margins. For instance, in box-girder and slab hollow decks, the mean values and their standard deviations are predominantly located within the blue and green regions, suggesting a robust dynamic design. Conversely, in lighter typologies such as filler beam or U-type decks, the mean values and the shaded regions sit significantly closer to the red saturated zone, indicating that a larger portion of the existing population of these types is susceptible to exceeding serviceability limits. The plots also confirm that for almost all typologies, the critical zone is concentrated at the intersection of low mass and low stiffness. The varied shapes and locations of the grey area across subplots highlight that deck typology is a primary factor in governing the dynamic reliability of the railway bridge network.

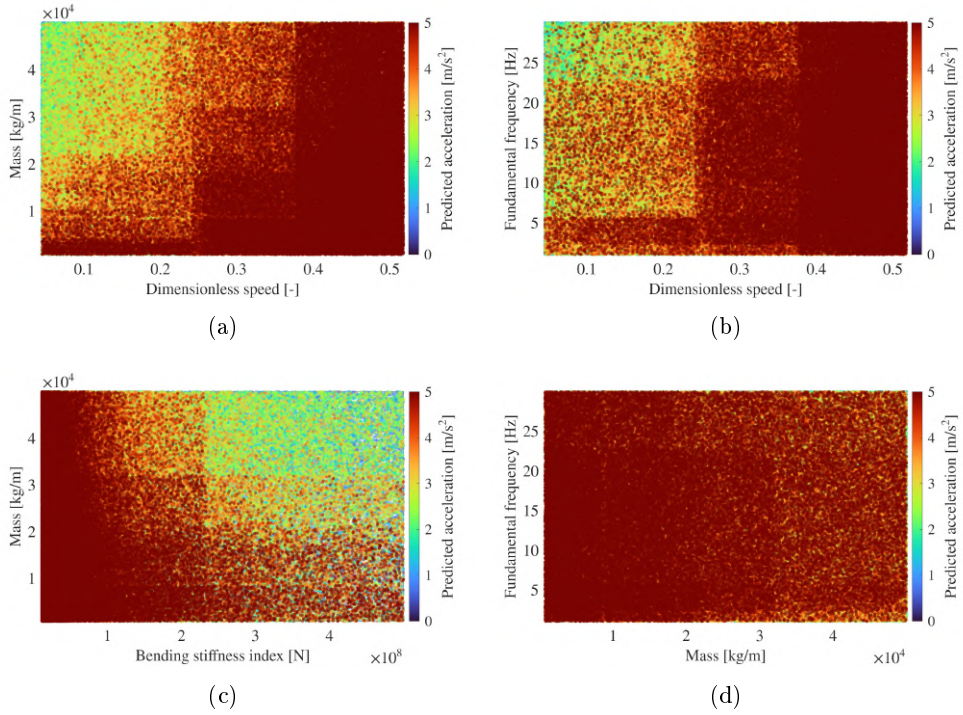

Figure 37: Parametric sensitivity and coupling analysis of vertical acceleration for simply-supported bridges: (a) influence of mass per unit length and (b) fundamental frequency as a function of dimensionless speed; (c) interaction between mass and bending stiffness; and (d) correlation between fundamental frequency and mass per unit length. The color scale is saturated at $5\,\mathrm{m/s^2}$.

In Figure 39 the dynamic response is evaluated by crossing mass per unit length and fundamental frequency for each deck typology of simply-supported bridges. This visualization reveals that resonance vulnerability is not uniformly distributed across frequencies. For most typologies, the critical red zone is significantly more pronounced at lower frequencies, where the interaction with typical train speeds and axle distances is more likely to trigger high-amplitude vibrations. The positioning of the mean values and the standard deviation relative to the frequency axis provides a direct measure of the spectral safety of each bridge type. In typologies such as box-girder and slab hollow, the database population is centred in frequency ranges that, combined with their high mass, keep the accelerations within the safe zones. In contrast, for filler beam, and U-type bridges, the grey area is not only situated in a low-mass region but also overlaps with frequency bands that are highly susceptible to high acceleration levels.

The analysis of these figures shows that low bending stiffness cannot be compensated by high mass, whereas a very stiff bridge can perform adequately even with limited mass. In general, low frequency bridges may perform well if sufficient mass is present, while high frequency ones could become problematic when associated with low masses. In short, a bridge having a low natural frequency is not necessarily a problem. The same train will induce resonance at a lower speed; however, if the bridge has sufficient mass (generally accompanied by sufficient stiffness), the response will not be high.

Within this framework, existing bridges performance varies significantly by typology. Filler beam bridges, characterized by very low stiffness and mass, tend to perform poorly

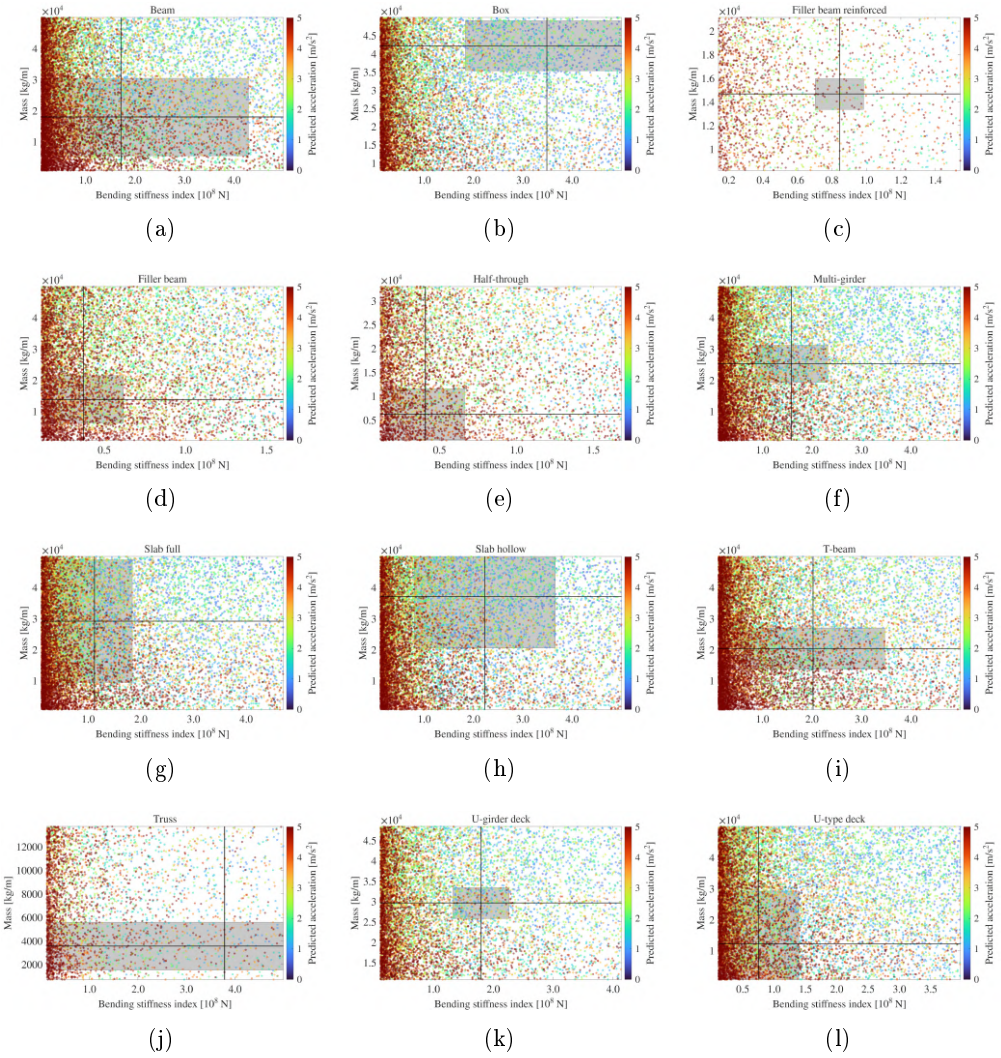

Figure 38: Analysis of vertical acceleration for simply-supported bridges as a function of mass and bending stiffness index for the different deck types. Black lines represent the mean values for the bridges in the database, while the shaded grey area denotes the range defined by the mean ± the standard deviation. The color scale is saturated at $5\,\mathrm{m/s^2}$.

despite exhibiting moderate natural frequencies (the mean being close to 10 Hz), and would require increases in both parameters. In contrast, box-girder bridges exhibit high bending stiffness (10 times higher than filler beams) and mass, resulting in low dynamic response and a very good performance, despite exhibiting low fundamental frequencies. Beam bridges present intermediate stiffness but relatively low mass, suggesting that an increase in mass could improve their behavior, while U-girder bridges occupy an intermediate position with satisfactory performance at low frequencies. Slab bridges show mixed behavior: full slabs resemble filler beams in their limitations, whereas hollow slabs, with greater stiffness for similar mass, are less prone to dynamic issues. Finally, half-through bridges, combining low stiffness with even lower mass, are inherently unfavorable from a dynamic performance standpoint.

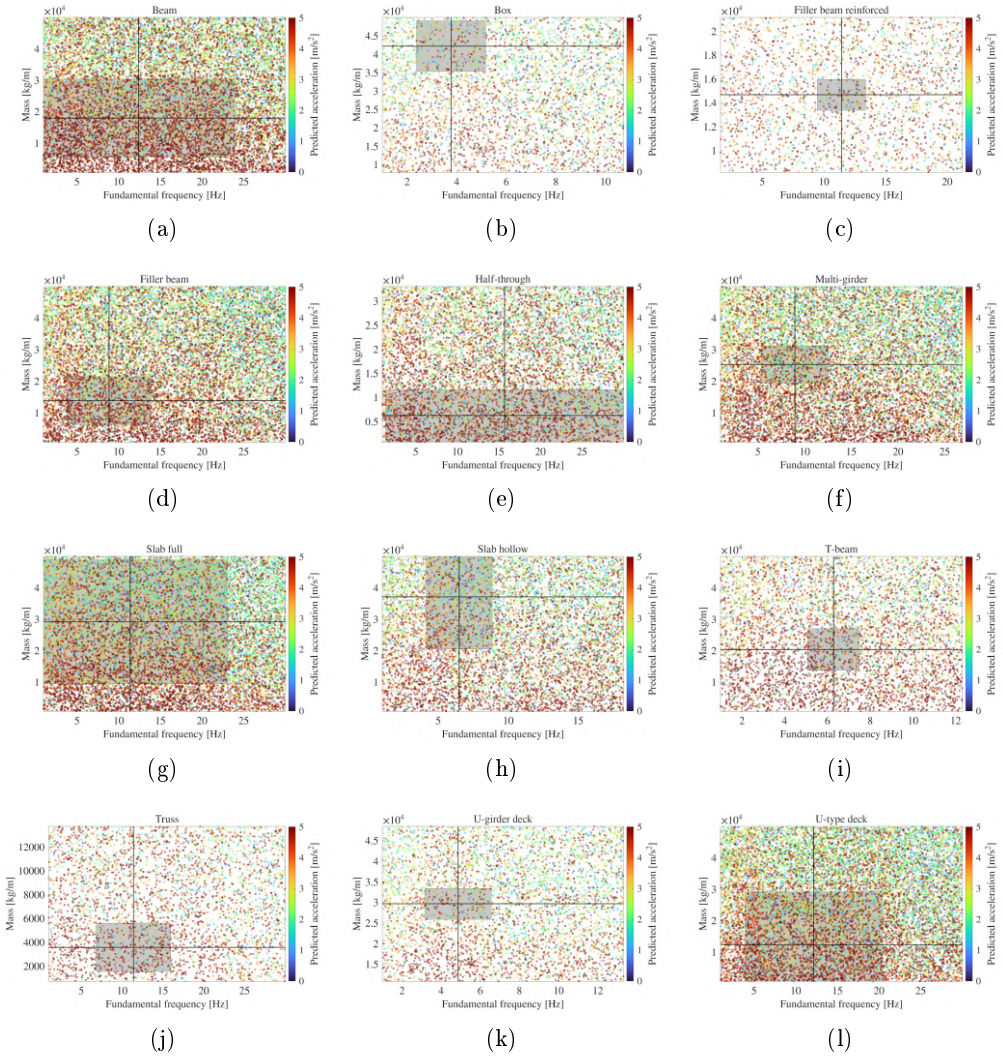

Figure 39: Analysis of vertical acceleration for simply-supported bridges as a function of mass and fundamental frequency for the different deck types. Black lines represent the mean values for the bridges in the database, while the shaded grey area denotes the range defined by the mean ± the standard deviation. The color scale is saturated at $5\,\mathrm{m/s^2}$.

The parametric sensitivity analysis for continuous bridges, presented in Figure 40, reveals a dynamic response structure that differs significantly from the patterns observed in simply-supported schemes. In the relationships involving dimensionless speed (Figures 40(a)) and 40(b)), structural continuity is shown to generate a much broader zone of low accelerations at moderate speeds, effectively shifting acceleration saturation towards more demanding operational ranges. From the interaction between mass and the bending stiffness index (Figures 40(c)), it can be concluded that continuous bridges exhibit a nearly vertical stiffness threshold that suggests the existence of a critical stiffness value below which the bridge is unable to meet serviceability criteria, regardless of its structural mass. Once this threshold is reached, the system undergoes an abrupt transition toward lower acceleration levels, showing that in the continuous bridges the

bending stiffness index is the primary filter for dynamic control. Finally, the relationship between fundamental frequency and mass (Figures 40(d)) shows that, despite the advantages of hyperstaticity, mass per unit length remains a governing factor for robust behaviour across the frequency spectrum, as the saturated red area persists dominantly in the lowest mass ranges.

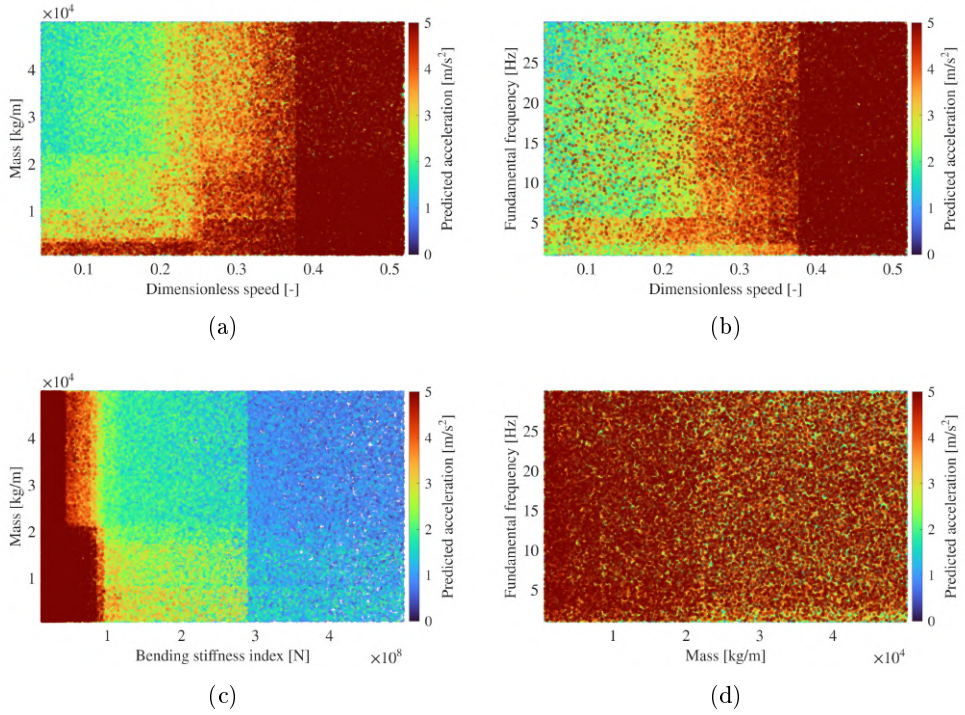

Figure 40: Parametric sensitivity and coupling analysis of vertical acceleration for continuous bridges: (a) influence of mass per unit length and (b) fundamental frequency as a function of dimensionless speed; (c) interaction between mass and bending stiffness; and (d) correlation between fundamental frequency and mass per unit length. The color scale is saturated at $5\,\mathrm{m/s^2}$.

The analysis by deck typology for continuous bridges, shown in Figure 41, confirms that the structural continuity provides a significantly higher safety margin across the full database. Unlike the simply-supported cases, the mean values (black lines) and the standard deviation areas (grey shaded zones) for almost all typologies are well positioned within the regions with low accelerations levels. This shift is particularly evident in the mass and bending stiffness interaction plots. For typologies like the multi-girder and U-girder deck, the existing bridges are designed in a range of stiffness that avoids high acceleration levels, even when their mass is relatively low. For continuous systems, the combination of extremely low mass and low stiffness represents a localized risk design area much smaller and less frequent than in simply-supported bridges.

The relationship between mass per unit length and fundamental frequency for continuous bridges is detailed by typology in Figure 42. A initial observation is the significant migration of the database population away from the lower-left critical zone. For nearly all typologies the average structural configuration sits within regions corresponding to accelerations well below the serviceability threshold. In contrast to the simply-supported case, where low mass causes exceedance regardless of frequency, the

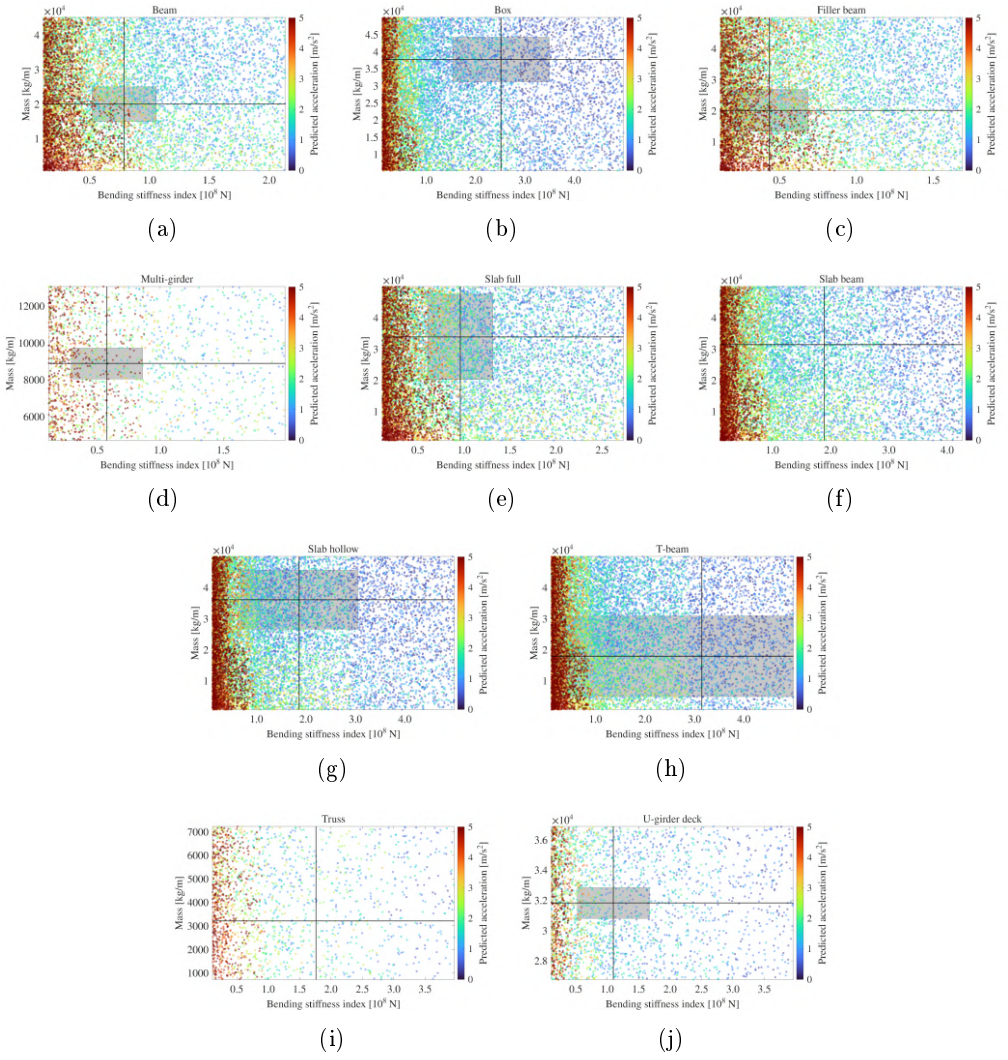

Figure 41: Analysis of vertical acceleration for continuous bridges as a function of mass and bending stiffness index for the different deck types. Black lines represent the mean values for the bridges in the database, while the shaded grey area denotes the range defined by the mean ± the standard deviation. The color scale is saturated at $5\,\mathrm{m/s^2}$.

continuity produces low accelerations at higher frequencies.

The parametric analysis for frame bridges, shown in Figures 43 to 45, reveals the highest level of dynamic robustness among all investigated structural systems. The rigid connection between the deck and the substructure increases both the global stiffness and the fundamental frequencies of the system. These structural designs imply that the database mean values are located beyond the visible limits of the axes. As shown in the global sensitivity maps (Figure 43), frame bridges exhibit lower acceleration levels compared to simply-supported and continuous bridges. The interaction between mass and bending stiffness (Figure 43(c)) identifies a critical stiffness threshold even lower than that of continuous bridges. The analysis by typology (Figures 44 and 45) shows that the grey areas are consistently located in the high-stiffness, high-frequency, and low-acceleration regions.

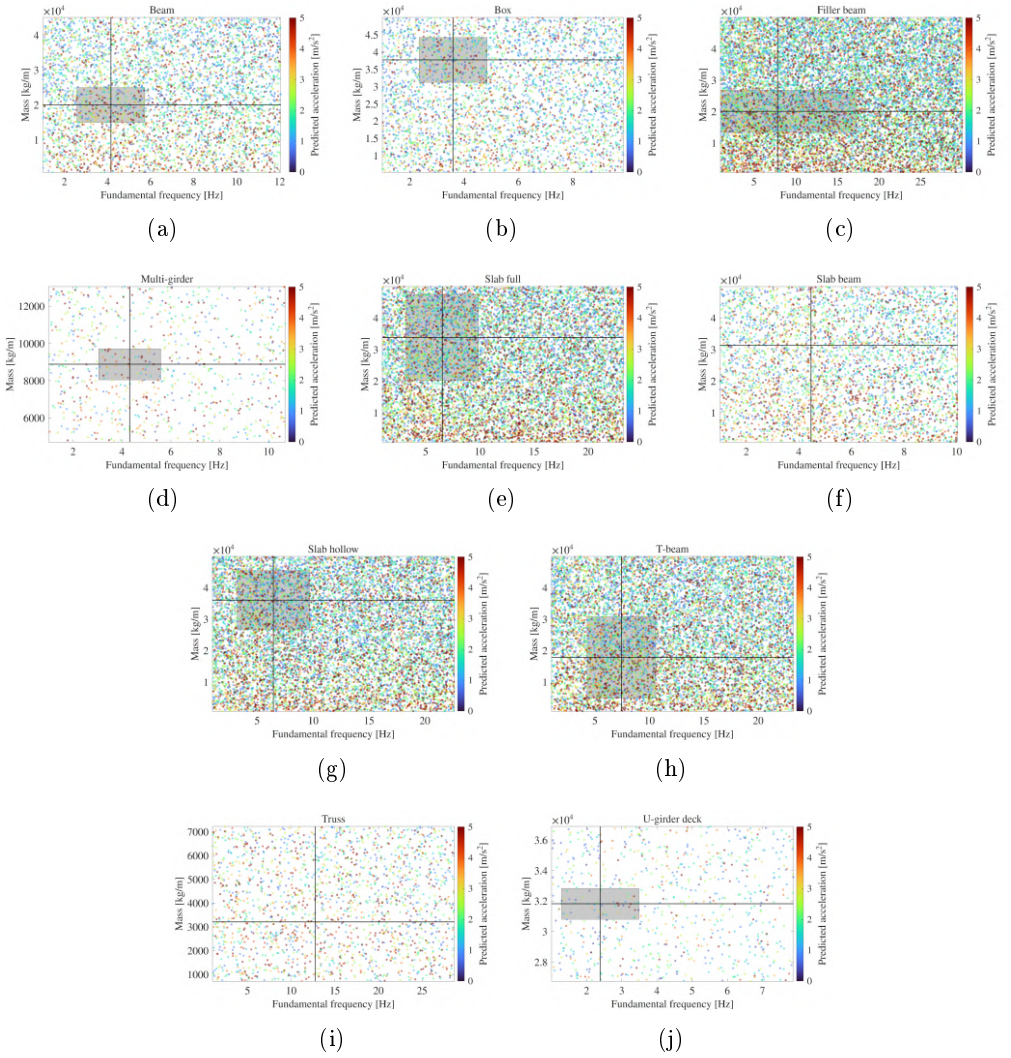

Figure 42: Analysis of vertical acceleration for continuous bridges as a function of mass and fundamental frequency for the different deck types. Black lines represent the mean values for the bridges in the database, while the shaded grey area denotes the range defined by the mean ± the standard deviation. The color scale is saturated at $5\,\mathrm{m/s^2}$.

The regression tree analysis presented in Figure 46 summarizes the dynamic trends previously identified in the parametric sensitivity maps. The results reinforce the clear distinction between the three primary structural families: simply-supported spans, continuous bridges, and frames. For the more robust configurations, such as frames and continuous systems, the tree confirms a high degree of stability, where serviceability limits are rarely exceeded. Conversely, for the simply-supported typology, the analysis highlights a more complex interaction. Increasing bending stiffness does not yield a linear improvement in performance; instead, for certain combinations of low mass and high stiffness, the system is prone to frequency tuning with the train's excitation. The tree validates that while structural continuity provides an inherently lower baseline for accelerations, the dynamic safety of simply-supported bridges remains critically dependent on a balanced ratio of mass and stiffness to avoid spectral overlap with traffic load

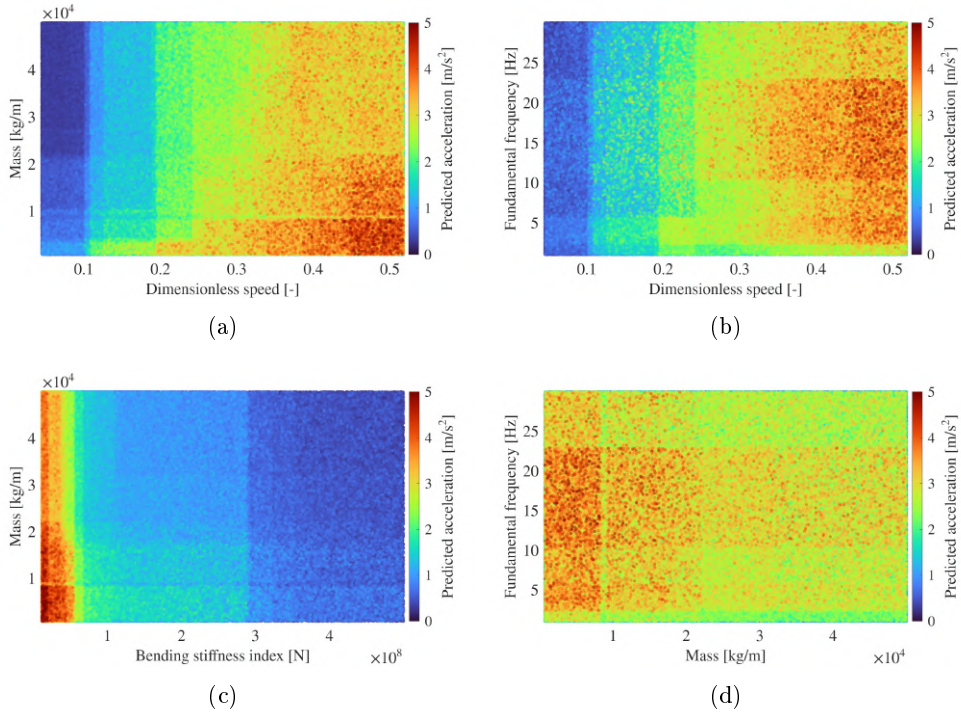

Figure 43: Parametric sensitivity and coupling analysis of vertical acceleration for frame bridges: (a) influence of mass per unit length and (b) fundamental frequency as a function of dimensionless speed; (c) interaction between mass and bending stiffness; and (d) correlation between fundamental frequency and mass per unit length. The color scale is saturated at $5\,\mathrm{m/s^2}$.

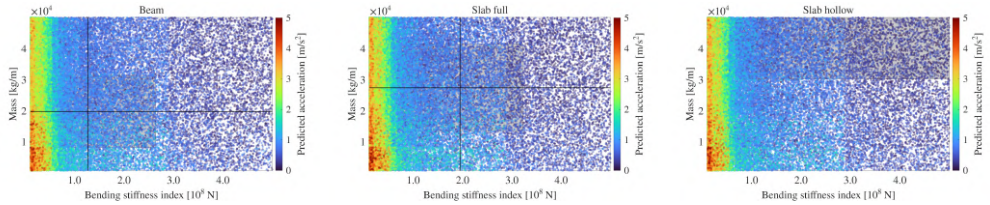

Figure 44: Analysis of vertical acceleration for frame bridges as a function of mass and bending stiffness index for the different deck types. Black lines represent the mean values for the bridges in the database, while the shaded grey area denotes the range defined by the mean ± the standard deviation. The color scale is saturated at $5\,\mathrm{m/s^2}$.

frequencies.

3.5 Predictive tool

Based on the developed RF LSBoost regression model, a design application (Figure 47) has been implemented to translate predictive results into structural engineering practice. It is important to emphasize that the predictive engine uses a single global model trained on the entire dataset, encompassing all structural configurations. This

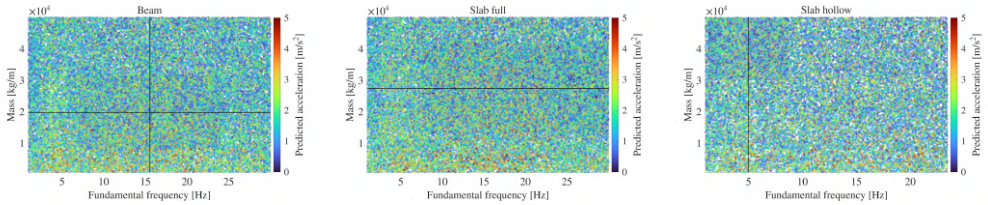

(a) (b) (c)

Figure 45: Analysis of vertical acceleration for frame bridges as a function of mass and fundamental frequency for the different deck types. Black lines represent the mean values for the bridges in the database, while the shaded grey area denotes the range defined by the mean ± the standard deviation. The color scale is saturated at $5\,\mathrm{m/s^2}$.

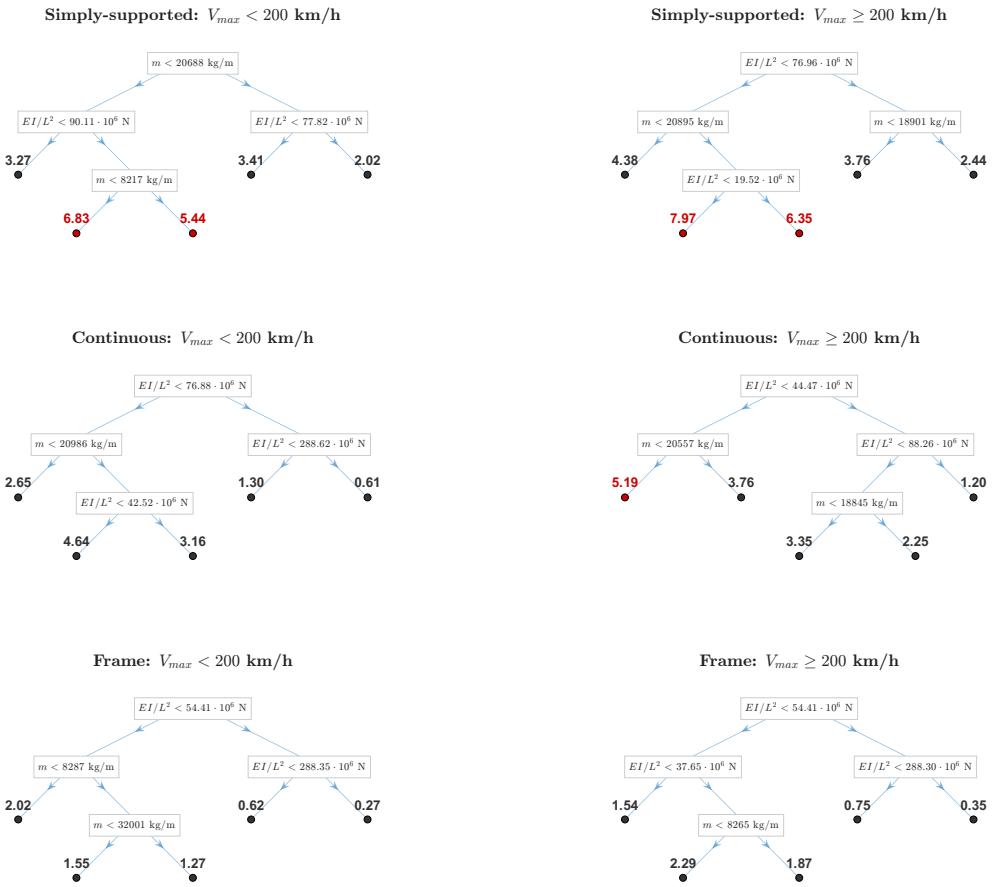

Figure 46: Regression tree for the multi-parametric prediction of vertical bridge acceleration. The terminal nodes show the mean predicted acceleration in $\mathrm{m/s^2}$. A color saturation is applied to acceleration values $\geq 5\mathrm{m/s^2}$.

approach ensures that the algorithm captures the shared underlying physical behaviour across different bridge typologies while maintaining high generalization capabilities. To transform the raw predictions into a reliable engineering value, a conservative margin is incorporated by adding the $RMSE$ specific to each structural configuration. This allows the tool to provide a design acceleration (a_{design}) that accounts for the historical uncertainty of the model for each specific category: $a_{design} = a_{pred} + RMSE_{config}$

(Table 1).

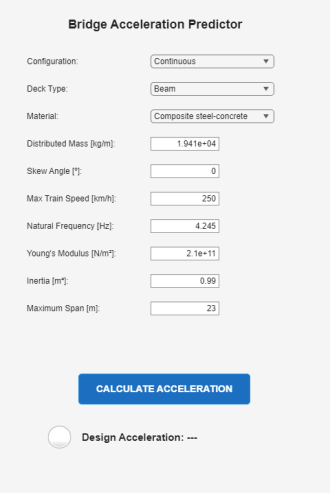

Figure 47: `Matlab` design application.

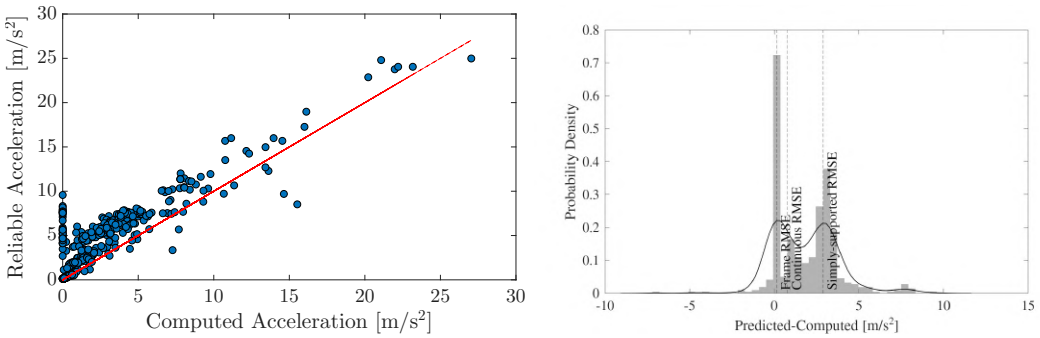

Figure 48: Performance evaluation of the proposed structural design tool: (a) scatter plot comparing the calculated design acceleration against the real computed acceleration. The red line represents the 1:1 identity line, and (b) the probability density function of the design errors. The $RMSE$ offsets for different bridge configurations are indicated by the vertical dashed lines.

Figure 48(a) shows the relation between the computed accelerations and the design accelerations calculated by the tool. By integrating the configuration-specific $RMSE$, the data points exhibit a deliberate positive shift. This shift effectively establishes a conservative envelope, ensuring that for more than 95% of the considered bridges the predicted design value equals or exceeds the computed acceleration, thereby minimizing the risk of underestimation in structural assessments. Figure 48(b) shows the probability density function of the design errors (defined as $a_{design} - a_{pred}$). The distribution shows a multimodal profile, a direct result of applying discrete $RMSE$ offsets across different structural typologies. The concentration of the probability in the positive region provides empirical evidence of the tool robustness. This statistical distribution indicates that the proposed methodology effectively provides a quantifiable safety buffer, shifting the model uncertainty towards a conservative, safe design range.

4 Conclusions

The integration of statistical analysis and machine learning applied to the prediction of the dynamic response of a vast railway bridge population has led to the following conclusions:

- The preliminary statistical assessment confirms that peak vertical accelerations are highly dependent on structural typology and fundamental frequency. Simply-supported bridges exhibit the highest susceptibility to resonance whereas continuous and frame structures show more controlled responses due to structural redundancy and high bending stiffness, respectively.
- Linear regression models are insufficient for precise acceleration prediction ($R^2 \approx 0.50$). Their failure to account for non-linear jumps in acceleration near resonant speeds makes them unreliable for railway bridge engineering applications.
- The optimized RF model achieved high predictive accuracy ($R^2 = 0.877$). The inclusion of the dimensionless speed as a top-ranked predictor proves that physical feature engineering is essential for allowing black-box models to capture the underlying spectral limit states of the structures.
- Categorical analysis reveals that while the RF model is extremely precise for frame structures ($RMSE = 0.071\,\mathrm{m/s^2}$), bridges with simply-supported spans remain the most challenging to predict due to their higher probability of experiencing significant response amplification.
- The proposed model may serve as an efficient screening tool for infrastructure managers. It allows for the rapid identification of at-risk bridges within large networks, enabling a predictive maintenance strategy.
- The dynamic response analysis shows that resonance vulnerability is mainly concentrated at low frequencies, where interaction with trains leads to higher accelerations. The relationship between mass, stiffness, and frequency is critical: low stiffness cannot be compensated by high mass, whereas high stiffness ensures good performance even with lower mass. Thus, low-frequency bridges can perform well if sufficient mass is present.
- For simply-supported bridges, performance varies by typology. Filler beam and half-through bridges perform poorly due to low stiffness and mass, while box-girder bridges perform well thanks to high stiffness. Other typologies show intermediate behaviour or could improve with increased mass or stiffness.
- In continuous bridges, structural continuity significantly improves dynamic behaviour, expanding low-acceleration regions. A critical stiffness threshold exists below which serviceability cannot be met regardless of mass. Once exceeded, accelerations decrease sharply, making stiffness the dominant parameter, although mass remains relevant at low ranges.
- Finally, frame bridges exhibit the best overall performance due to their high stiffness and natural frequencies, resulting in the lowest acceleration levels and greatest dynamic robustness.

- The design application transfers the RF model by incorporating typology-specific $RMSE$ offsets to derive conservative design accelerations (a_{design}). This implementation transforms the predictive output into a safety-oriented envelope, providing a quantifiable margin that minimizes the risk of underestimation in real infrastructure assessments.

References

[1] INF TSI. Technical specifications for interoperability relating to the 'infrastructure' subsystem of the rail system in the European Union. Official Journal of the European Union, Brussels, Belgium; 2019.

[2] LOC & PAS TSI. Technical specification for interoperability relating to the 'rolling stock - locomotives and passenger rolling stock' subsystem of the rail system in the European Union. Official Journal of the European Union, Brussels, Belgium; 2019.

[3] European Committee for Standardization. EN 15528. Railway applications - Line categories for managing the interface between load limits of vehicles and infrastructure. Brussels, Belgium; 2021.

[4] European Committee for Standardization. EN 1990-Annex A2. Eurocode 0: Basis of structural design - Annex 2: Application for bridges (normative). Brussels, Belgium; 2001.

[5] European Committee for Standardization. EN 1991-2. Eurocode 1: Actions on structures - Part 2: Traffic loads on bridges. Brussels, Belgium; 2003.

[6] Montenegro PA, Carvalho H, Ribeiro D, Calçada R, Tokunaga M, Tanabe M, et al. Assessment of train running safety on bridges: A literature review. Engineering Structures. 2021;241:112425. Available from: https://www.sciencedirect.com/science/article/pii/S0141029621005757.

[7] Jesus AH, Dimitrovová Z, Silva MAG. A statistical analysis of the dynamic response of a railway viaduct. Engineering Structures. 2014;71:244-59. Available from: https://www.sciencedirect.com/science/article/pii/S0141029614002259.

[8] Monti G, Rabi RR, Marella L, Proietti ST. Data-driven decision support system for the safety management of railway bridge networks. Reliability Engineering & System Safety. 2025;262:111202. Available from: https://www.sciencedirect.com/science/article/pii/S095183202500403X.

[9] Collings D. Estimates of the useful lifetime of bridges using a generated database. Proceedings of the Institution of Civil Engineers - Civil Engineering. 2025;178(3):184-92. Available from: https://www.sciencedirect.com/science/article/pii/S0965089X25000199.

[10] Shen L, Hong Y, Li L, Wang H, Pu Q. Physics-enhanced prediction model for shear bearing capacity of railway bridge piers based on flexural-shear coupling theory. Engineering Structures. 2025;343:120993. Available from: https://www.sciencedirect.com/science/article/pii/S0141029625013847.

[11] Elnahla M, Guo Y, Atadero RA. A new Gaussian process regression-based approach to leverage non-destructive evaluation data in bridge deterioration prediction models. Engineering Structures. 2026;351:121988. Available from: https://www.sciencedirect.com/science/article/pii/S014102962502379X.

[12] Bayane I, Leander J, Karoumi R. An unsupervised machine learning approach for real-time damage detection in bridges. Engineering Structures. 2024;308:117971. Available from: https://www.sciencedirect.com/science/article/pii/S0141029624005339.

[13] Le Nguyen K, Pham TM, Nguyen K, Banihashemi S. Automation in dynamic analysis and generative design of prestressed concrete railway bridge infrastructures. Computers in Industry. 2026;176:104440. Available from: https://www.sciencedirect.com/science/article/pii/S0166361526000072.

[14] ERRI D214/RP9 PB. Rail bridges for speeds > 200 km/h. European Rail research Institute, The Netherlands; 1999.

[15] Romero A, Moliner E, Martínez-Rodrigo MD, Galvín P. Analytical solution for dynamic response of multi-span bridges under moving loads: an efficient method based on time-discrete analysis using sinc interpolation. Applied Mathematical Modelling. 2026;151:116491. Available from: https://www.sciencedirect.com/science/article/pii/S0307904X25005657.

[16] Nguyen K, Goicolea JM. CALDINTAV: A simple software for dynamic analysis of high-speed railway bridges using the semi-analytical modal method. Software Impacts. 2024;22:100700. Available from: https://www.sciencedirect.com/science/article/pii/S2665963824000885.

[17] Museros P, Moliner E, Martínez-Rodrigo MD. Free vibrations of simply-supported beam bridges under moving loads: Maximum resonance, cancellation and resonant vertical acceleration. Journal of Sound and Vibration. 2013;332(2):326-45. Available from: https://www.sciencedirect.com/science/article/pii/S0022460X12006293.